# Boundary Layer Dissipation and the Nonlinear Interaction of Equatorial Baroclinic and Barotropic Rossby Waves

Joseph A. Biello[1] & Andrew J. Majda
Courant Institute of Mathematical Sciences, 251 Mercer St, New York, NY 10012

Received _____; accepted _____

**ABSTRACT**

Two layer equatorial primitive equations for the free troposphere in the presence of a thin atmospheric boundary layer and thermal dissipation are developed here. An asymptotic theory for the resonant nonlinear interaction of long equatorial baroclinic and barotropic Rossby waves is derived in the presence of such dissipation. In this model, a self-consistent asymptotic derivation establishes that boundary layer flows are generated by meridional pressure gradients in the lower troposphere and give rise to degenerate equatorial Ekman friction. That is to say, the asymptotic model has the property that the dissipation matrix has one eigenvalue which is nearly zero: therefore the dynamics rapidly dissipates flows with pressure at the base of the troposphere and creates barotropic/baroclinic spin up/ spin down. The simplified asymptotic equations for the amplitudes of the dissipative equatorial barotropic and baroclinic waves are studied by linear theory and integrated numerically. The results indicate that although the dissipation slightly weakens the tropics to midlatitude connection, strong localized wave packets are nonetheless able to exchange energy between barotropic and baroclinic waves on intraseasonal time scales in the presence of baroclinic mean shear. Interesting dissipation balanced wave-mean flow states are discovered through numerical simulations. In general, the boundary layer dissipation is very efficient for flows in which the barotropic and baroclinic components are of the same sign at the base of the free troposphere whereas the boundary layer dissipation is less efficient for flows whose barotropic and baroclinic components are of opposite sign at the base of the free troposphere.

*Subject headings:* equatorial Rossby waves; atmospheric boundary layer; amplitude equations

## 1. Introduction

The meridional exchange of energy between the midlatitudes and equatorial regions is a topic of considerable significance for understanding global teleconnection patterns from the tropics to the midlatitudes. Several authors have used linearized two layer primitive equations on a $\beta$-plane in order to describe the interaction of long equatorial baroclinic Rossby waves and long equatorial barotropic Rossby waves. The linear theory of the primitive equations in the zonal long wave limit yield two sets of waves. The first are weakly dispersive, zonally long, equatorially trapped baroclinic Rossby waves. For a dry

[1]Corresponding author, email: biello@cims.nyu.edu, phone (212) 998-3185

gravity wave speed of $50\,\mathrm{ms}^{-1}$ the fastest of these travel at $-16.6\,\mathrm{ms}^{-1}$ (see Majda (2003) for a comprehensive discussion). The primitive equations also have linear solutions which correspond to equatorial barotropic Rossby waves with a significant midlatitude projection. In the long wave limit these waves, too, are dispersionless and travel westward at a speed proportional to their wavelength squared.

Equatorial baroclinic Rossby waves provide a description of planetary scale phenomena in the tropics. Similarly, equatorial barotropic Rossby waves describe phenomena linked with potentially significant connections between the tropics and midlatitudes. Several authors (see Webster (1971; 1981; 1982), Kasahara and Silva Dias (1986), Hoskins and Jin (1991), Wang and Xie (1996), Lim and Chang (1981; 1986) and Hoskins and Yang (2000)) have studied these waves in the context of midlatitude connections to the tropics. These studies have found that nearly dispersionless long equatorial baroclinic Rossby waves can exchange significant energy with barotropic waves at midlatitudes in the presence of vertical and meridional mean shears.

With the benefit of this intuition Majda and Biello (2003) and Biello and Majda (2003) recently have derived a long wave theory describing the nonlinear interaction of equatorial baroclinic waves and barotropic waves in the presence of zonal mean barotropic shears and zonal mean vertical shears. The partial differential equations of the theory describe waves longer than 5000 km in the zonal direction and 1500 km meridionally. The theory admits waves of amplitude on the order of $5\,\mathrm{ms}^{-1}$ near the equator interacting with zonal mean velocities and vertical shears of about the same strength. In these studies it was shown that the presence of vertical, baroclinic shear allows for significant energy exchange between the tropically confined baroclinic waves and barotropic waves with significant midlatitude projection on timescales on the order of fifteen days. While detailed comparison with observations of the present theories (this work and that of Majda and Biello (2003) and Biello and Majda (2003) ) will be presented elsewhere, equatorially trapped Rossby waves with a significant barotropic component are often observed propagating westward in the eastern Pacific (Kiladis and Wheeler (1995) and Wheeler, Kiladis and Webster (2000)).

Important additional effects not considered by Majda and Biello (2003) and Biello and Majda (2003) are dissipative mechanisms arising from radiative cooling and atmospheric boundary layer drag. In this paper we shall systematically incorporate these mechanisms in the asymptotic theory of Majda and Biello (2003) and Biello and Majda (2003) following the resonant long wave theory that they developed for equatorial baroclinic an barotropic waves: hereafter we refer to these papers collectively as MB. The models we develop here show that, due to boundary layer dissipation, various anomalies on time scales of ten days can strengthen upper troposphere flow while simultaneously weakening flow at the base of the troposphere. This feature is part of the observational record of anomalies such as the intraseasonal oscillation (see Yanai et al. (2000)).

A two layer tropospheric model with weak Newtonian cooling is coupled to a

convectively well mixed, thin barotropic boundary layer (see Neelin (1988), Wang and Li (1993) and Moskowitz and Bretherton (2000) for the origin of similar boundary layer models). Following MB, resonantly interacting baroclinic and barotropic tropospheric long waves are studied. Here the mean tropical climatology is represented by fairly weak (order $5\text{ms}^{-1}$ barotropic and baroclinic shears which are appropriate for the tropics. Though the boundary layer dissipation times are relatively small for the (twelve day) intraseasonal time scales of interest here, the boundary layer is thin in comparison to the troposphere. This combination allows for a longer relaxation time in the troposphere due to boundary layer dissipation and leads in a systematic fashion to equatorial Ekman friction which is described by a degenerate linear operator. Since radiative cooling is weak, it is straightforward to incorporate in the higher order terms of the asymptotic theory of MB.

In section 2 we describe the basic two layer model with a well mixed barotropic boundary layer. In 2.1 the long wave asymptotics is described while in 2.2 the linear theory of low Froude number flows is described in detail. Section 2.3 assembles these pieces into a systematic long wave theory of equatorial baroclinic and barotropic Rossby waves in the presence of boundary layer dissipation. In section 3 amplitude equations are constructed for resonantly interacting baroclinic and barotropic wavetrains. The new linear dissipation terms are evaluated in section 3.1 and the normal form rescaling from MB is provided in 3.2. The linear theory of mean flows and waves is described in section 4. Section 5 provides a series of numerical examples which illustrate the nonlinear behavior of the amplitude equations with dissipation included. Solitary waves solutions are used in 5.1 to demonstrate the breaking of vertical symmetry by dissipation. Sections 5.2 and 5.3 revisit the examples of midlatitude to tropics wave energy exchange that were studied by MB. Section 5.4 considers the long time evolution to a nonlinear balanced state. We conclude in section 6 with a brief discussion of our results.

## 2. Atmospheric boundary layer and radiative damping effects on long equatorial baroclinic and barotropic waves

We shall systematically incorporate boundary layer drag and thermal dissipation in the description of resonantly interacting equatorial baroclinic and barotropic long waves. To this end we consider a standard two layer $\beta$-plane model describing the free troposphere, whose vertical extent is $0 \leq z \leq H_T$. In addition, at the base of the free troposphere there is assumed to be a well mixed, barotropic boundary layer with extent $-z_B \leq z \leq 0$. The velocity profile as a function of height is sketched in figure 1.

The equatorial baroclinic and barotropic waves in the free troposphere are described by much the same equations previously considered by Majda and Biello (2003), and Biello and Majda (2003). The nonlinear equations for the interaction of barotropic, $\vec{v}_0$, and baroclinic, $\vec{v}_1$, modes in the free troposphere can be derived in standard fashion (Neelin and Zeng

(2000), Majda and Shefter (2001) ) from a two vertical mode Galerkin truncation of the Boussinesq equations on the $\beta$-plane with rigid lid boundary conditions with the form

$$\begin{aligned} \vec{v} =& \vec{v}_0(x,y) + \vec{v}_1(x,y)\sqrt{2}\cos\left(\frac{\pi z}{H_T}\right) \\ p =& p_0(x,y) + p_1(x,y)\sqrt{2}\cos\left(\frac{\pi z}{H_T}\right) \end{aligned} \tag{1}$$

where $p_j$ are the pressures associated with each mode and $H_T = 16.75\,\mathrm{km}$ is the troposphere thickness. Using the gravity wave speed, $c = \frac{H_T \bar{N}}{\pi}$ determined by the Brunt-Vaisala frequency, $\bar{N} = 10^{-2}s^{-1}$, we consider the non-dimensionalized equations with the unit of meridional and zonal length measured by the equatorial Rossby radius, $L_E = (c/\beta)^{1/2}$ and time given by $T_E = (c\beta)^{-1/2}$. Velocity and pressure are nondimensionalized by $c$ and $c^2$, respectively. The natural non-dimensional vertical length scale in is measured by $H = H_T/\pi \approx 5\,\mathrm{km}$ while the units for nondimensional vertical velocity, $w$, are $H/T_E$. Following MB, the standard values associated with dry wave propagation of a baroclinic heating mode with

$$c = 50\,\mathrm{ms}^{-1},\ T_E = 8.3\,\mathrm{hrs},\ L_E = 1500\,\mathrm{km} \tag{2}$$

will be used below to demonstrate various qualitative effects of the nonlinear coupling. Hereafter all functions and variables are nondimensional.

The equations

$$\frac{\bar{D}\vec{v}_0}{\bar{D}t} + y\,\vec{v}_0^{\perp} + \nabla\cdot\,(\vec{v}_1 \otimes \vec{v}_1) = -\nabla p_0 - \frac{1}{2}(\nabla\cdot\vec{v}_0)\vec{v}_0 \tag{3}$$

$$\nabla\cdot\,\vec{v}_0 = -\Delta_B\,(\nabla\cdot\,\vec{v}_B) \tag{4}$$

$$\frac{\bar{D}\,\vec{v}_1}{\bar{D}t} + y\,\vec{v}_1^{\perp} + (\vec{v}_1\cdot\nabla)\,\vec{v}_0 = -\nabla p_1 - \frac{1}{2}(\nabla\cdot\vec{v}_0)\vec{v}_1 \tag{5}$$

$$\frac{\bar{D}\,p_1}{\bar{D}t} + \nabla\cdot\,\vec{v}_1 = -\hat{d}_\theta p_1 - \sqrt{2}\Delta_B\,(\nabla\cdot\vec{v}_B) - \frac{1}{2}(\nabla\cdot\vec{v}_0)p_1 \tag{6}$$

$$\frac{D^B\,\vec{v}_B}{Dt} + y\,\vec{v}_B^{\perp} = -\nabla\left(p_0 + \sqrt{2}p_1\right) - \hat{d}\,\vec{v}_B - \frac{1}{2}\vec{v}_B\,(\nabla\cdot\vec{v}_B). \tag{7}$$

describe a barotropic, $\vec{v}_0$, and baroclinic, $\vec{v}_1$, velocity field where $\vec{v}_j = (u_j, v_j)$, $\vec{v}_j^{\perp} = (-v_j, u_j)$, $p_j$ are functions of the horizontal variable, $(x,y)$ alone and all the vector derivatives involve only horizontal differentiation. Here and elsewhere in the paper the transport operator $\frac{\bar{D}}{Dt} = \frac{\partial}{\partial t} + \vec{v}_0\cdot\nabla$, represents advection by the barotropic mode. The quantity $\vec{v}_B = (u_B, v_B)$ represents the velocity in the boundary layer and the advective derivative in the boundary layer refers to the horizontal boundary layer velocity, $\frac{D^B}{Dt} = \frac{\partial}{\partial t} + \vec{v}_B\cdot\nabla$. A Newtonian cooling term, $\hat{d}_\theta\,p_1$ appears in equation (6) and will be further discussed below.

The boundary layer has thickness $z_B$ and the ratio

$$\Delta_B \equiv \frac{z_B}{H_T} \tag{8}$$

is the fundamental nondimensional quantity appearing in equations (3) - (6) and we shall exploit the fact that it is a small parameter. The profile of horizontal velocity in dimensional variables as a function of height in the troposphere is shown in figure 1 (a). It is clear that the barotropic mode corresponds to a vertically homogeneous horizontal mean wind in the free troposphere whereas the baroclinic mode yields a net vertical shear. For further discussion of the equations describing the dynamics of the equatorial baroclinic and barotropic waves the reader is referred to Wang and Xie (1996) and MB.

In this model, the atmospheric boundary layer at the base of the troposphere is assumed to be convectively well mixed and therefore barotropic. Similar boundary layer models have been used previously in the context of tropical baroclinic waves (Neelin (1988), Wang and Li (1993) and Moskowitz and Bretherton (2000)). The boundary layer has nondimensionalized vertical extent $-\pi\Delta_B \leq z \leq 0$, horizontal velocity $\vec{v}_B$ and it is assumed that all of the frictional dissipation occurs there through the term $\hat{d}\,\vec{v}_B$ in equation (7). Equation (7) and the terms which couple the boundary layer velocity to the free troposphere in equations (3)-(6) are derived by assuming that the barotropic boundary layer is coupled to the troposphere through the continuity of vertical velocity and pressure across the fixed interface, $z = 0$. The boundary layer pressure on the right hand side of equation (7), $p_B = p_0 + \sqrt{2}p_1$, is simply the sum of the baroclinic and barotropic pressure at the base of the free troposphere according to equation (1). A vertical velocity which decreases linearly with height is thereby imparted on the barotropic flow in the free troposphere above the boundary layer which, in turn, is the source of the divergence of $\vec{v}_0$ in equation (4). In fact, the non-dimensional vertical velocity in the troposphere, $w$, associated with a boundary layer velocity, $\vec{v}_B$, and baroclinic velocity, $\vec{v}_1$ is

$$w = -\Delta_B\,(\pi - z)\,\nabla\cdot(\vec{v}_B) - \sqrt{2}\,\nabla\cdot(\vec{v}_1)\sin(z), \quad 0 \leq z \leq \pi \tag{9}$$

where the first term in (9) is the barotropic vertical velocity which vanishes at the top of the troposphere, $z = \pi$, and the second, the baroclinic vertical velocity, vanishes at the top and bottom of the troposphere. The vertical velocity as a function of height due to each of these components is shown in figure 1 (b). Note that as in other boundary layer models for engineering flows, the horizontal velocity is permitted to jump discontinuously across the boundary layer through the boundary conditions which match only pressure and vertical velocity.

The interface at $z = 0$ has non-zero vertical velocity and should therefore sustain interfacial waves. Strictly speaking the boundary condition across the interface between the free troposphere and the barotropic boundary layer should be continuity of pressure and continuity of normal velocity across $z = \eta(x, y, t)$ where $\eta$ describes this free interface. In addition the evolution of $\eta$ is described by a kinematic constraint relating its advective derivative to the vertical velocity at the interface. A Boussinesq model describing a free troposphere interacting with a barotropic boundary layer can be written down with these assumptions and, in the absence of dissipation, the non-linear interactions in this model would automatically conserve energy. However, the vertical Galerkin truncation which

separates such a model into a barotropic and first baroclinic requires a basis which conforms to the dynamic boundary at $z = \eta$. Such an approach has been carried out systematically by Ripa (1995) in a somewhat simpler context.

Since the boundary layer is both barotropic and thin in comparison to the free troposphere, $\Delta_B \ll 1$, both the vertical velocity at the interface and the deviation of the interface from its equilibrium, $\eta$ are small. Therefore the boundary condition can effectively be applied at $z = 0$ with the deviations leading to higher order nonlinearities. The quadratic nonlinear terms on the right hand side of equations (3) - (7) are added in a somewhat ad hoc fashion so that nonlinear advection in the absence of dissipation conserves energy. Therefore they model the effect of the variation of boundary layer thickness which is otherwise not included when assuming a stationary interface. Since the terms contribute only higher order effects in the asymptotic expansions developed here their specific form is not relevant for any of the results in this paper.

Recall that the ratio of boundary layer thickness to the height of free the troposphere is $\Delta_B = z_B/H_T$ and we will exploit the fact that the boundary layer is thin in comparison to the troposphere. In practice, the height of the well mixed tropical boundary layer varies from 0.5 to 1.0 km (Wang and Li (1993), Moskowitz and Bretherton (2000)). Thus, the reasonable values of boundary layer thickness and troposphere height $z_B = 1.0$ km, $H_T = 16.75$ km yield

$$\Delta_B \approx 0.06 \tag{10}$$

which we shall use as a representative value for purposes of illustration throughout the rest of this paper. A boundary layer dissipation timescale can be calculated using a turbulent drag coefficient of $C_D = 10^{-3}$ (Majda and Shefter (2001)) , typical turbulent velocities of $2 - 5\text{ms}^{-1}$ and the boundary layer thickness. This yields a dissipation time of order one day in the boundary layer so that the nondimensional drag coefficient is

$$\hat{d} \approx 0.3. \tag{11}$$

with $T_E \approx 8.3$ hrs. The model constructed in the following sections explicitly illustrates that the combination of a thin boundary layer with a one day relaxation time sets a longer boundary induced decay time in the free troposphere in a highly anisotropic fashion.

The effect of thermal dissipation is included through a Newtonian cooling term in the baroclinic pressure equation (5). Thermal damping is observed to occur on roughly 18 - 20 day timescales yielding

$$\hat{d}_\theta \approx 0.02 \tag{12}$$

as a representative value used below.

As remarked the equations (3-7) conserve energy in the absence of boundary layer drag and thermal dissipation, otherwise the energy decays. The energy relation can be readily

derived and yields

$$\begin{aligned}\frac{d\,E}{dt} =& \frac{1}{2}\int_D \left[|\vec{v}_0|^2 + |\vec{v}_1|^2 + p_1^2 + \Delta_B|\vec{v}_B|^2\right]\, dx\, dy \\ =& -\Delta_B \int_D |\vec{v}_B|^2\, dx\, dy - d_\theta \int_D p_1^2\, dx\, dy.\end{aligned} \tag{13}$$

The integrals are taken over the two dimensional $\beta$-plane which is periodic in $x$ (zonally) and bounded in $y$ (meridionally).

### 2.1. Zonal long wave scaling

Our theory is concerned with tropospheric flows which vary slowly in the zonal direction and evolve on longer timescales than the equatorial time, $T_E$. We shall consider flows whose meridional variations occur on Rossby deformation lengthscales, $L_E$, while zonal variations occur on a longer length $L$ and evolve on timescales, $T$, which are long compared to $T_E$. Since $\Delta_B$ is small, the barotropic velocity field is primarily solenoidal with a potentially significant projection at midlatitudes. Furthermore, it is well known that baroclinic flows in the equatorial wave guide have primarily zonal propagation with a limited extent of a few thousand kilometers in the north-south direction but a much larger east-west scale varying over the entire 40000 km circumference of the globe (Wang and Xie, (1996), MB). These considerations suggest that we consider flows whose meridional velocity is small compared to the zonal velocity. As in MB (also see §9.3 of Majda (2003)) define the small parameter, $\delta$ as follows,

$$\frac{L_E}{L} = \delta,\ \frac{T_E}{T} = \delta,\ |v| = \delta|u|, \tag{14}$$

for $\delta \ll 1$ and seek solutions of the equations in (3) and (5) for the free troposphere of the form

$$\begin{aligned} p_j &= p_j\left(\delta x, y, \delta t\right) \\ u_j &= u_j\left(\delta x, y, \delta t\right) \\ v_j &= \delta v_j\left(\delta x, y, \delta t\right) \end{aligned} \tag{15}$$

for $j = 0, 1$.

Boundary layer flow is driven by pressure gradients in the overlying troposphere. In the long wave approximation for the free troposphere the solutions have meridional pressure gradients which dominate zonal gradients. In the boundary layer linear theory, the pressure forcing is balanced against the Coriolis effect and boundary layer dissipation. Therefore, for the flow in the boundary layer we also assume meridional variations over a long length scale but we do not require meridional velocities to be $O(\delta)$ smaller than zonal velocities. Therefore we seek solutions of the boundary layer velocity of the form

$$\vec{v}_B = \vec{v}_B\left(\delta x, y, \delta t\right). \tag{16}$$

It is the divergence of the boundary layer dissipation which couples the boundary flow to the free troposphere baroclinic and barotropic equations. According to the scaling hypothesis in equation (16), the meridional and zonal components of the boundary layer flow are of the same order, yet the long wave scaling means that zonal variations are $O(\delta)$ smaller than meridional variations. Therefore the divergence of the boundary layer velocity is dominated by the meridional derivative of the meridional boundary layer velocity; the zonal derivative of the zonal component is $O(\delta)$ smaller. It will become clear that, in this approximation, only the meridional component of the boundary layer velocity plays a role in the dissipation of the waves in the free troposphere. These assumptions differ from the ones in Moskowitz and Bretherton (2000) where linearized boundary layer equations are simplified through long wave asymptotics.

With these approximations, the long-wave scaled equations as in MB emerge. With the ansatz in equations (15) and (16) the barotropic and baroclinic equations for the free troposphere from equations (3) and (5) become

$$\begin{aligned}
\frac{\bar{D}u_0}{\bar{D}t} - yv_0 + \nabla\cdot(u_1\vec{v}_1) + (p_0)_x &= \frac{\Delta_B}{2\delta}\left[(v_B)_y + \delta\,(u_B)_x\right]\,u_0 \\
yu_0 + (p_0)_y + \delta^2\left[\frac{\bar{D}v_0}{\bar{D}t} + \nabla\cdot(v_1\vec{v}_1)\right] &= \frac{\Delta_B}{2}\left[(v_B)_y + \delta\,(u_B)_x\right]\,v_0 \\
(u_0)_x + (v_0)_y &= -\frac{\Delta_B}{\delta}\left[(v_B)_y + \delta\,(u_B)_x\right]
\end{aligned} \tag{17}$$

and

$$\begin{aligned}
\frac{\bar{D}u_1}{\bar{D}t} + \vec{v}_1\cdot\nabla u_0 - yv_1 + (p_1)_x &= \frac{\Delta_B}{2\delta}\left[(v_B)_y + \delta\,(u_B)_x\right]\,u_1 \\
yu_1 + (p_1)_y + \delta^2\left[\frac{\bar{D}v_1}{\bar{D}t} + \vec{v}_1\cdot\nabla v_0\right] &= \frac{\Delta_B}{2}\left[(v_B)_y + \delta\,(u_B)_x\right]\,v_1 \\
\frac{\bar{D}p_1}{\bar{D}t} + \nabla\cdot\vec{v}_1 &= \frac{\Delta_B}{\delta}\left[(v_B)_y + \delta\,(u_B)_x\right]\,\left(\frac{p_1}{2} - \sqrt{2}\right) - \frac{\hat{d}_\theta}{\delta}p_1.
\end{aligned} \tag{18}$$

Finally, the long wave scaled barotropic boundary layer equations are

$$\begin{aligned}
\delta\left[\frac{\partial u_B}{\partial t} + \left(u_B^2\right)_x + \left(p_0 + \sqrt{2}p_1\right)_x\right] + \left(u_B\,v_B\right)_y &= y\,v_B - \hat{d}\,u_B \\
\delta\left[\frac{\partial v_B}{\partial t} + \left(u_B\,v_B\right)_x\right] + \left(v_B^2\right)_y + \left(p_0 + \sqrt{2}p_1\right)_y &= -y\,u_B - \hat{d}\,v_B.
\end{aligned} \tag{19}$$

Together, these equations are the Long Wave Scaled Equations for Equatorial Baroclinic and Barotropic waves (LWSEBB, see MB) in the presence of thermal and boundary layer dissipation. To avoid cumbersome notation, the arguments of the variables in equations (15) and (16) are written implicitly in the LSWEBB and are still denoted by $x, y, t$.

### 2.2. Leading order asymptotics in a low Froude number expansion

The tropospheric zonal velocities in equations (17) and (18) are measured in units of the propagation speed of a dry baroclinic mode, $50\,\mathrm{ms}^{-1}$ from equation (2). Typical mean winds and vertical shears at the equator are on the order of $5-10\,\mathrm{ms}^{-1}$. As in MB this motivates a small amplitude solution of the long wave equations (17)-(19) of order $\epsilon$, where $\epsilon$, the Froude number, is the ratio of typical wind velocities to the dry wave propagation velocity, $c$. Combining equations (15), (16) with this low Froude number assumption we construct asymptotic solutions of equations (3),(5) and (7) with the form

$$\begin{aligned} p_j &= \epsilon p_j^{(1)}\left(\delta x, y, \delta t, \delta\epsilon t\right) + \epsilon^2 p_j^{(2)}\left(\delta x, y, \delta t, \delta\epsilon t\right) + \ldots \\ u_j &= \epsilon u_j^{(1)}\left(\delta x, y, \delta t, \delta\epsilon t\right) + \epsilon^2 u_j^{(2)}\left(\delta x, y, \delta t, \delta\epsilon t\right) + \ldots \\ v_j &= \delta\epsilon v_j^{(1)}\left(\delta x, y, \delta t, \delta\epsilon t\right) + \delta\epsilon^2 v_j^{(2)}\left(\delta x, y, \delta t, \delta\epsilon t\right) + \ldots \\ \vec{v}_B &= \epsilon \vec{v}_B^{(1)}\left(\delta x, y, \delta t, \delta\epsilon t\right) + \epsilon^2 \vec{v}_B^{(2)}\left(\delta x, y, \delta t, \delta\epsilon t\right) + \ldots \end{aligned} \tag{20}$$

where $j = 0, 1$ as before. A wind velocity of $5\,\mathrm{ms}^{-1}$ yields the reasonable value of $\epsilon = 0.1$; we shall fix $\epsilon = 0.1$ in the examples for purposes of illustration as in MB. In the subsequent section a distinguished limit balancing dispersion and nonlinearity will be sought requiring $\delta^2 = \epsilon$ but for the time being we shall not make such a restriction in order to maintain generality. As in MB, the relation $\delta^2 = \epsilon$ yields the value $\delta = 0.31$ in equations (15), (16) as well as for (17), (18) and (19); thus meridional variations are of order 1500 km while zonal variations are of order $\delta^{-1}L_E \approx 5000\,\mathrm{km}$.

Substituting the scalings of equation (20) into equations (17), (18), (19) the leading order in $\epsilon$ and $\delta$ yields the linear theory of barotropic and baroclinic waves in addition to the boundary layer theory. Since we are not interested in waves which damp strongly within a wave travel time we make the mild assumption that

$$\frac{\Delta_B}{\delta} = o\left(1\right) \quad \text{and} \quad \frac{\hat{d}_\theta}{\delta} = o\left(1\right). \tag{21}$$

The typical values of $\Delta_B$ and $\hat{d}_\theta$ given in equations (10) and (11) fall well within these restrictions. The resultant linear theory describes long equatorial barotropic waves

$$\begin{aligned} \left(u_0\right)_t - y v_0 + \left(p_0\right)_x &= 0 \\ y u_0 + \left(p_0\right)_y &= 0 \\ \left(u_0\right)_x + \left(v_0\right)_y &= 0 \end{aligned} \tag{22}$$

and long equatorial baroclinic waves

$$\begin{aligned} \left(u_1\right)_t - y v_1 + \left(p_1\right)_x &= 0 \\ y u_1 + \left(p_1\right)_y &= 0 \\ \left(p_1\right)_t + \left(\nabla \cdot \vec{v}_1\right) &= 0 \end{aligned} \tag{23}$$

each of which are in meridional geostrophic balance and decoupled from the boundary layer. The equations in (22) and (23) are simply the linear barotropic long-wave equations and the linear equatorial long-wave equation, respectively, discussed by Heckley and Gill (1984), Majda (2003) and MB.

The linear barotropic long-wave equation (22) has the well known dispersion relation, $\omega_{BT} = -\frac{k}{l^2}$, with corresponding dispersionless Rossby wave train solutions,

$$\psi = -B^S\left(x - c_{BT}t\right)\sin\left(ly\right) - B^A\left(x - c_{BT}t\right)\cos\left(ly\right), \quad c_{BT} = -\frac{1}{l^2} \tag{24}$$

for any wavenumber $l$. The velocity components are $(u_0, v_0) = (-\psi_y, \psi_x)$ and the superscripts "S" and "A" denote zonal flows which are symmetric or antisymmetric about the equator, respectively.

Similarly, the linear equatorial long wave equation, (23), has dispersionless equatorial Rossby wavetrain solutions (Heckley and Gill (1984), Majda (2003))

$$\begin{pmatrix} p \\ u \\ v \end{pmatrix} = \begin{pmatrix} -\frac{A_m(x-c_mt)}{\sqrt{2}}\left(D_{m-1}(\sqrt{2}y) + \frac{D_{m+1}(\sqrt{2}y)}{(m+1)}\right) \\ \frac{A_m(x-c_mt)}{\sqrt{2}}\left(D_{m-1}(\sqrt{2}y) - \frac{D_{m+1}(\sqrt{2}y)}{(m+1)}\right) \\ -\left(\frac{2}{2m+1}\right)\frac{\partial A_m(x-c_mt)}{\partial x}D_m(\sqrt{2}y) \end{pmatrix} \tag{25}$$

for any integer $m > 0$ where $D_m(\eta)$ are the parabolic cylinder functions and

$$c_m = -\frac{1}{2m+1}. \tag{26}$$

The baroclinic waves have symmetric zonal flows about the equator for $m$ odd and antisymmetric zonal flows for $m$ even and decay exponentially away from the equator.

From equations (19) and (20), the leading order boundary layer equations are the equatorial Ekman equations,

$$\begin{aligned} yv_B - \hat{d}u_B &= 0 \\ yu_B + \hat{d}v_B &= -\left(p_0 + \sqrt{2}p_1\right)_y. \end{aligned} \tag{27}$$

These are simply inhomogeneous linear algebraic equations which can be readily solved in terms of the tropospheric pressure or zonal velocity

$$\begin{aligned} u_B &= -\frac{y\left(p_0 + \sqrt{2}p_1\right)_y}{\left(\hat{d}^2 + y^2\right)} = \frac{y^2\left(u_0 + \sqrt{2}u_1\right)}{\left(\hat{d}^2 + y^2\right)} \\ v_B &= -\frac{\hat{d}\left(p_0 + \sqrt{2}p_1\right)_y}{\left(\hat{d}^2 + y^2\right)} = \frac{\hat{d}\,y\,\left(u_0 + \sqrt{2}u_1\right)}{\left(\hat{d}^2 + y^2\right)}. \end{aligned} \tag{28}$$

The second equalities in (28) arise from the meridional geostrophic balances in equations (22) and (23) and, using equation (1), indicate that the boundary layer velocity is proportional to the total zonal velocity at the base of the free troposphere. In fact, the zonal component of the boundary layer velocity is in the same direction as the total zonal component of the velocity at the base of the troposphere. On the other hand, the meridional component of the boundary layer flow points away from the equator (divergent) for westerly winds and toward the equator (convergent) for easterlies. In particular, the meridional boundary layer velocity is in the opposite direction of the meridional component of the pressure gradient (as is the zonal component).

The variation with $y$ of the coefficients in equation (28) is also interesting. Due to the long zonal scale and long time approximation and the consequent meridional geostrophic balance in the troposphere, both the meridional and zonal component of the boundary layer velocity vanish along the equator, $y = 0$. Furthermore, meridional flows are stronger than zonal flows at the equator yet as $|y| \to \infty$, $u_B \to (u_0 + \sqrt{2}u_1)$ and the meridional boundary layer flow tends to zero; the roles of the two components are reversed. Clearly, since both coefficients in equation (28) are functions of the parameter $y/\hat{d}$ the non-dimensional parameter, $\hat{d}$, sets the scale for this transition in the relative strengths in the velocities.

### 2.3. LWSEBB equations in the presence of a thin boundary layer

Under the assumption of weak dissipation, equation (21), long wavelength linear barotropic and baroclinic waves are nearly dispersionless and do not dissipate. This suggests that there is a distinguished limit where the inclusion of a thin barotropic boundary layer with order one dissipation effectively provides linear dissipation of momentum to the long waves in the troposphere on a long timescale, $\tau \equiv \delta\epsilon t$ (refer to the equations 20). In particular we assume that the leading order barotropic divergence term is $O(\epsilon^2)$ so that $\frac{\Delta_B}{\delta} \sim \epsilon$; the same will be true of the Newtonian cooling. In order to single out small terms in the equatorial baroclinic/barotropic equations, we define new order one parameters

$$\bar{\Delta} \equiv \frac{\Delta_B}{\epsilon\delta} \quad \text{and} \quad \bar{d_\theta} \equiv \frac{\hat{d}_\theta}{\epsilon\delta}. \tag{29}$$

which describe the ratio of the boundary layer thickness to troposphere height and the small thermal dissipation coefficient.

In order to have weak dispersive effects compete with nonlinearity in these long wave solutions (as in Boyd (1980), Patoine and Warn (1981), Majda and Biello (2003)) the zonal long-wave parameter, $\delta$, in equations (17), (18) and (19) and the amplitude, $\epsilon$, in equation (20) will be balanced and satisfy $\delta^2 = \epsilon$. MB discussed how the reasonable value of $\epsilon = .1$ allows zonal velocities of order $5\,\mathrm{ms}^{-1}$ and, with $\delta^2 = \epsilon$, zonal variation on scales of order $L_E\,\delta^{-1} \approx 5000\,\mathrm{km}$; thus the relation $\delta^2 = \epsilon$ is physically realistic. With this choice of small parameters, one unit of the long timescale, $\tau$, equals 11 days.

Using the physically relevant values from MB discussed earlier, $\epsilon = 0.1$, $\delta = \sqrt{\epsilon} \approx 0.31$, and the boundary layer thickness and thermal dissipation from equations (10) and (11), $\Delta_B \approx 0.06$, $\hat{d}_\theta \approx 0.02$ the rescaled parameters take on the values

$$\bar{\Delta} \approx 2 \quad \text{and} \quad \bar{d}_\theta \approx 0.67, \tag{30}$$

both of which are order one so the assumptions in equation (29) are reasonable.

We have assembled all the pieces to construct solutions of the equatorial barotropic/baroclinic equations in the free troposphere in the presence of the dissipation from the boundary layer and thermal dissipation. Using the scalings described in equations (20) and (29), the multiple timescales $t$ (which is the $\delta$ rescaled original time), the slower timescale $\tau = \delta\epsilon t$ needed in section 3 while including only the leading order effects from the boundary layer, the long wave equatorial barotropic equations become

$$\begin{aligned} \frac{\bar{D}u_0}{\bar{D}t} - yv_0 + \nabla\cdot(u_1\vec{v}_1) + (p_0)_x + \epsilon u_{0,\tau} &= \mathcal{O}(\epsilon^3) \\ yu_0 + (p_0)_y + \delta^2\left[\frac{\bar{D}v_0}{\bar{D}t} + \nabla\cdot(v_1\vec{v}_1)\right] + \epsilon v_{0,\tau} &= \mathcal{O}(\delta\epsilon^3) \\ (u_0)_x + (v_0)_y &= -\bar{\Delta}\epsilon\,(v_B)_y + \mathcal{O}(\epsilon^2) \end{aligned} \tag{31}$$

and the long wave equatorial baroclinic equations become

$$\begin{aligned} \frac{\bar{D}u_1}{\bar{D}t} - yv_1 + \vec{v}_1\cdot\nabla u_0 + (p_1)_x + \epsilon u_{1,\tau} &= \mathcal{O}(\epsilon^3) \\ yu_1 + (p_1)_y + \delta^2\left[\frac{\bar{D}v_1}{\bar{D}t} + \vec{v}_1\cdot\nabla v_0\right] + \epsilon v_{1,\tau} &= \mathcal{O}(\delta\epsilon^3) \\ \frac{\bar{D}p_1}{\bar{D}t} + \nabla\cdot\vec{v}_1 + \epsilon p_{1,\tau} &= -\epsilon\left(\bar{d}_\theta p_1 + \sqrt{2}\bar{\Delta}\,(v_B)_y\right) + \mathcal{O}(\epsilon^3). \end{aligned} \tag{32}$$

Here the low Froude number scaling in equation (20) has been used to evaluate the order of the neglected terms. Note that a power of $\delta$ has been canceled in the first and last equations in (31) and (32). Also, as in equations (17), (18) and (19), the convention that the zonal coordinate, $x$, and time, $t$, are the original variables rescaled by $\delta$ and that the fields have order one variation on these scales is employed. The meridional boundary layer velocity, $v_B$, is given as a function of the baroclinic and barotropic velocities by equation (28), thus closing equations (31) and (32).

Since the barotropic velocity is solenoidal at leading order, it is convenient to use a stream function and a potential through the Helmholtz decomposition

$$\vec{v}_0 = \nabla^\perp\psi(\delta x, y, \delta t, \delta\epsilon t) + \nabla\phi(\delta x, y, \delta t, \delta\epsilon t). \tag{33}$$

Without canceling $\delta$'s the nearly incompressible constraint on the velocity field from equation (3) is

$$\nabla\cdot\vec{v}_0 = -\delta\epsilon\bar{\Delta}(v_B)_y \tag{34}$$

and substituting equation (33) into (34) yields

$$\delta^2\phi_{xx} + \phi_{yy} = -\bar{\Delta}\,\delta\epsilon\,(v_B)_y \tag{35}$$

again the zonal variable, $x$ refers to the long zonal scale. Notice that zonal potential flows are order $\delta$ smaller than meridional flows and, furthermore, $\phi_y$ is order $\delta\epsilon$ smaller than $v_B$ so to lowest order the meridional velocity due to potential flow is given by

$$\phi_y = -\bar{\Delta}\,\delta\epsilon v_B. \tag{36}$$

This equality expresses the fact vertically integrated meridional mass flux in the boundary layer is balanced by an opposite flux in the troposphere. We can now recast equations (31) using the stream function. Recognize that, since the velocity from the potential is already order $\delta\epsilon$ smaller than the other terms, we need only consider its lowest order, linear contribution. The lowest order contribution of the potential terms enters at order $\epsilon$ and arises from the linear term in the velocity equation associated with the $\beta$-effect. Therefore taking the curl of the first two equations in (31) yields the barotropic vorticity equation

$$\begin{aligned} &\frac{\bar{D}\,\psi_{yy}}{\bar{D}t} + \psi_x - \nabla\cdot\Big((\vec{v}_1\,u_1)_y\Big) + \\ \delta^2&\left\{\frac{\bar{D}\,\psi_{xx}}{\bar{D}t} + \nabla\cdot\left((\vec{v}_1\,v_1)_x\right)\right\} + \epsilon\psi_{yy,\tau} = \bar{\Delta}\epsilon\,(y\,v_B)_y + \mathcal{O}(\epsilon^3,\delta^2\epsilon^2) \end{aligned} \tag{37}$$

The boundary layer zonal velocity is given explicitly in terms of the pressure or troposphere velocity through equation (28). The equations (32) and (37) constitute the Dissipative Long Wave Scaled Equatorial Baroclinic Barotropic equations (DLWSEBB).

## 3. Amplitude equations for DLWSEBB

Amplitude equations for the undamped LWSEBB have been derived and discussed in detail by Majda and Biello (2003) and Biello and Majda (2003). We shall not reproduce the derivations here but instead outline the procedure and focus on the derivation of the new terms in the amplitude equations.

Using the distinguished limit of dispersion balanced nonlinearity, we set $\delta^2 = \epsilon$ for the remainder of this discussion. The asymptotic series of equation (20) is substituted into the dissipative long wave scaled equatorial baroclinic/ barotropic equations, (32) and (37), and the resultant equations are solved at each order in $\epsilon$. At lowest order, $\epsilon^1$, the linear barotropic long-wave equations (22) and the linear equatorial long-wave equations (23) emerge. As already discussed, their solutions are the dispersionless barotropic Rossby wavetrains of equation (24) and equatorial baroclinic Rossby wavetrains of equation (25).

Only resonantly interacting long waves will yield nontrivial solvability conditions for the amplitude equations. For a fixed $m$, the dispersionless packets in (24) and (25) are

resonant for a barotropic mode with meridional wavelength, $L_*$ with $l = \frac{2\pi}{L_*} L_E$ provided that

$$\begin{aligned} & c_{BT}(L_*) = c_m \implies l = \sqrt{2m+1} \\ \text{or} \quad & \frac{L_*}{L_E} \equiv L = \frac{2\pi}{\sqrt{2m+1}} \end{aligned} \tag{38}$$

for $m = 1, 2, ....$ With the gravity wave speed, $c = 50\,\mathrm{ms}^{-1}$ and $L_E = 1500\,\mathrm{km}$ from (2) the dimensional meridional wavelengths of the resonant barotropic Rossby waves are approximately

$$\begin{aligned} L_* &\cong 3.6\, L_E = 5440\,\mathrm{km} \quad \text{for} \quad m = 1 \\ L_* &\cong 2.8\, L_E = 4200\,\mathrm{km} \quad \text{for} \quad m = 2. \end{aligned} \tag{39}$$

The wave packets are referred to a frame moving at the resonant wave speed, $-16.7$ ms$^{-1}$ and $-10$ ms$^{-1}$ for $m = 1, 2$, respectively. Fixing the resonant values of $l$ we proceed to second order.

As in MB, the ultimate goal here is to derive simplified dynamics for the interaction of barotropic and equatorially trapped baroclinic waves in spherical geometry. Below we make several approximations in deriving the asymptotic models. First, spherical geometry is replaced by an equatorial $\beta$-plane geometry and, as in MB, the flows on the $\beta$-plane are assumed to be confined to a finite channel domain defined by no penetration boundary conditions at $y = \pm L_*$, i.e.

$$v|_{y=\pm L_*} = 0. \tag{40}$$

Wang and Xie (1996) have established the important fact that linear theory for coupled equatorial baroclinic/barotropic Rossby waves on the $\beta$-plane, in the long wave regime with baroclinic and barotropic mean shears is an excellent approximation to similar waves in spherical geometry with boundaries at $y = \pm L_*$ where $L_* \leq 4L_E$. The values of $L_*$ in equation (39) are compatible with this. Also, Longuet-Higgins (1968) has shown that the $\beta$-plane approximation is an excellent one for equatorially trapped baroclinic waves on the sphere.

Note that as in MB, the symmetric barotropic Rossby mode with amplitude $B^S$ in equation (24) exactly satisfies the boundary condition in equation (40). The equatorial Rossby wave trains in equation (25) do not exactly satisfy these boundary conditions at $y = \pm L_*$ but do so withing exponentially small errors since the dominant contribution from the eigenfunctions involve parabolic cylinder functions, $D_m(y)$, with the decay factor, $e^{-y^2/2}$; for $y = L_*$ from equations (39), $e^{-y^2/2} \approx 0.0015,\ 0.019$ for $m = 1, 2$, respectively. Thus, while strictly speaking one should use the more cumbersome exact finite channel equatorial baroclinic eigenfunctions to exactly satisfy equation (40), for simplicity in discussion we use instead the simplified formulas in equation (25) for the equatorial Rossby waves. For additional reasons this is an especially good approximation because, according to equation

(20) the meridional flows are already scaled to be weaker in magnitude. As a check, note that the free tropospheric flows in the figures in MB and presented below in the present paper all visually satisfy equation (40) at $y = \pm L_*$ even though the approximation in equation (25) is utilized. Also, as in the formulas computed in (3.10) and (3.12) from MB, the integrals in the asymptotic interaction coefficients between barotropic and baroclinic waves including the boundary layer are extended from the domain, $|y| \leq L_*$, to the entire integration range, $-\infty < y < \infty$. Thus, the interaction coefficients in the asymptotic model are calculated approximately in this fashion. As regards MB, this last approximation is a negligible one for the basic interaction coefficients since the ambiguous error terms from (3.10) and (3.12) of MB all involve *squares* of parabolic cylinder functions integrated against oscillating periodic functions for $|y| > L_*$ and, as shown above, the Gaussians are already small in amplitude at $|y| = L_*$. Here similar approximations are also used for the new boundary layer contributions. In addition, the leading order Ekman flows, $\phi_y$, in equation (36) are picked self-consistently from equation (28) and do not satisfy the boundary condition in equation (40) at $y = \pm L_*$, but only in the limit, $|y| \to \infty$. Finally, the antisymmetric Rossby wave contribution, $B^A$ in equation (24) has been carried along below to discuss the symmetries of the interaction through Ekman friction even though it solves stress-free boundary conditions rather than no-normal flow at $y = \pm L_*$ from equation (40).

At second order in $\epsilon$ (using equation (20) and $\delta^2 = \epsilon$) the equation governing the stream function from (37) and the baroclinic velocity and pressure from (32) are the linear long wave equations in (22) and (23) with inhomogeneities arising from the first order terms. These inhomogeneous terms are simply functions of the first order wave packets and, since they travel at the baroclinic long wave speed, are resonant with the linear operator. The resonance gives rise to secular growth of the second order fields and must be removed by projection of the nonlinear terms onto the adjoint eigenfunctions of the linear problem. Since the linear equations are self-adjoint, the adjoint eigenfunctions are given by the meridional structure of the baroclinic wave packet in equation (25) and each of the meridional structures of the barotropic wave packet from equation (24). As discussed in detail in MB (and generalized in Biello and Majda (2003)), multiplying the second order equations by each of these adjoint eigenfunctions and integrating in $y$ results in the amplitude equations

$$\begin{aligned} r_A A_\tau - D_A A_{xxx} + \alpha (A\, B^S)_x &= \Lambda_{BC} \\ r_B B^S_\tau - D_B B^S_{xxx} + \alpha A A_x &= \Lambda_S \\ r_B B^A_\tau - D_B B^A_{xxx} &= \Lambda_A \end{aligned} \tag{41}$$

for each value of $m = 1, 2, \ldots$. The amplitudes $A(x - c_m t, \tau)$, $B^S(x - c_m t, \tau)$ and $B^A(x - c_m t, \tau)$ with $\tau = \epsilon t$ are defined in equations (25) and (24) for packets of barotropic and equatorial baroclinic Rossby waves under the conditions in equation (38). The coefficients $\Lambda$ arise from the dissipation terms on the right hand sides of equations (32) and

(37) and are given by

$$\begin{aligned}
\Lambda_{BC} &= -\int_{-\infty}^{\infty} \hat{p}\left(\bar{d}_\theta\, p_1^{(1)} + \sqrt{2}\bar{\Delta}\left(v_B^{(1)}\right)_y\right)\, dy \\
\Lambda_S &= -\bar{\Delta}\int_{-L}^{L} l\cos(ly)\; y\; v_B^{(1)}\, dy \\
\Lambda_A &= \bar{\Delta}\int_{-L}^{L} l\sin(ly)\; y\; v_B^{(1)}\, dy
\end{aligned} \tag{42}$$

where $\hat{p}$ is the meridional structure of the pressure component of the baroclinic waves, the first entry in equation (25),

$$\hat{p} = -\frac{1}{\sqrt{2}}\left(D_{m-1} + \frac{D_{m+1}}{(m+1)}\right) \tag{43}$$

and the meridional flow in the boundary layer is given explicitly in terms of the zonal flow at the base of the troposphere by

$$v_B = \frac{\hat{d}\, y\, \left(u_0 + \sqrt{2}u_1\right)}{\left(\hat{d}^2 + y^2\right)}. \tag{44}$$

MB derive amplitude equations which are those of equation (41) without any dissipation terms, $\Lambda$. The specific forms of the coefficients on the left hand side of equation (41) can be found there. We remark that the form of the asymptotic expansion allows for zonal mean barotropic and baroclinic shears which have the same meridional structure as the waves; simply the zonal means of $A$, $B^S$ and $B^A$. Since waves of different meridional structure (i.e. different $m$) are unable to resonantly interact, one need only consider equations (41) for a fixed $m$ in isolation from the other modes.

Biello and Majda (2003) consider the more general case when the background shear has arbitrary meridional structure, in particular a meridional structure opposite to that of the underlying waves. To fix ideas, let us consider a baroclinic mean zonal shear composed of the meridional eigenfunctions of the $m = 1$ and $m = 2$ baroclinic waves and a zonal mean barotropic shear with meridional structure consisting of $l = \sqrt{3}$ and $l = \sqrt{5}$ sines and cosines. In such instances the equations derived by MB allow for the exchange of wave energy to $l = \sqrt{3}$ antisymmetric barotropic waves from symmetric barotropic waves and baroclinic waves through coupling with the $l = \sqrt{5}$ barotropic and $m = 2$ baroclinic mean shears. Similarly $l = \sqrt{5}$ antisymmetric barotropic waves resonantly exchange wave energy by coupling through the $l = \sqrt{3}$ zonal mean barotropic and $m = 1$ mean baroclinic shears. The amplitude equations derived by MB conserve the zonal mean flows and thus waves of different meridional structure (i.e. $m = 1, 2, ...$) can be considered in isolation from the rest. However the presence of dissipation allows the evolution - in particular the decay - of the

zonal mean shears. A complete description of the waves in this case would require both the $m = 1$ and $m = 2$ equations derived in MB with the addition of the dissipation terms, $\Lambda$. It is a straightforward exercise to add the dissipation terms to the equations considered by Biello and Majda (2003) and allow the amplitudes of the mean shears to evolve under dissipation. This level of generality is not exploited here but it is interesting for potential applications.

### 3.1. Evaluation of the dissipation coefficients

In this section we show that the component of the dissipation vector $\mathbf{\Lambda}$ arising from the boundary layer has the structure of a nearly degenerate symmetric matrix acting on the vector of wave amplitudes

$$\mathbf{\Lambda} = \begin{bmatrix} \Lambda_{BC} \\ \Lambda_S \\ \Lambda_A \end{bmatrix} = -\bar{\Delta} \begin{bmatrix} \hat{\gamma}_{11} & \hat{\gamma}_{12} & \hat{\gamma}_{13} \\ \hat{\gamma}_{12} & \hat{\gamma}_{22} & 0 \\ \hat{\gamma}_{13} & 0 & \hat{\gamma}_{33} \end{bmatrix} \begin{bmatrix} A \\ B^S \\ B^A \end{bmatrix}. \tag{45}$$

We point out that physically the degeneracy means that there exists a combination of barotropic and baroclinic velocities such that

$$v_B = 0 \Longrightarrow u_0 + \sqrt{2}u_1 = 0 \tag{46}$$

is satisfied exactly in the DLWSEBB. However, the amplitude equations (41) project the baroclinic and barotropic flows onto meridional eigenfunctions such that equation (46) cannot be satisfied exactly for all $y$. A full description of the boundary layer dissipation would require the complete bases to describe $u_0$ and $u_1$ in which case the dissipation matrix in equation (45) would be infinite and exactly degenerate (with an infinite null space). The matrix in equation (45) is simply a truncation of the infinite matrix and as such retains only a near degeneracy.

The component of the dissipation arising from the thermal dissipation only acts on the baroclinic waves and has the form

$$\Lambda_{BC}^{Thermal} = -\bar{d_\theta}\hat{\gamma}_\theta A. \tag{47}$$

It is straightforward to calculate the thermal dissipation coefficient from equation (42)

$$\hat{\gamma}_\theta = \int_{-\infty}^{\infty} \hat{p}^2 \, dy. \tag{48}$$

In order to calculate the coefficients of the boundary layer dissipation matrix it is convenient to define the kernel arising from the Ekman pumping

$$F(y;\hat{d}) \equiv \hat{d}\,\frac{(y/\hat{d})^2}{1+(y/\hat{d})^2}. \tag{49}$$

After integrating by parts, using the geostrophic balance from equation (23), $\hat{p}_y = -y\hat{u}$, and the definition of the baroclinic meridional eigenfunction from equation (25)

$$\hat{u} = \frac{1}{\sqrt{2}} \left( D_{m-1}(\sqrt{2}y) - \frac{D_{m+1}(\sqrt{2}y)}{(m+1)} \right) \tag{50}$$

it is straightforward to show that the dissipation matrix, $\hat{\Gamma} = (\hat{\gamma}_{ij})$, from equation (45) is symmetric and does not couple the two barotropic components. The explicit values of the coefficients are

$$\begin{aligned}
\hat{\gamma}_{11} =& 2 \int_{-\infty}^{\infty} F(y;\hat{d})\, \hat{u}^2 \, dy \\
\hat{\gamma}_{12} =& \sqrt{2} \int_{-\infty}^{\infty} F(y;\hat{d})\, l \cos(ly)\, \hat{u} \, dy \\
\hat{\gamma}_{13} =& -\sqrt{2} \int_{-\infty}^{\infty} F(y;\hat{d})\, l \sin(ly)\, \hat{u} \, dy \\
\hat{\gamma}_{22} =& \int_{-L}^{L} F(y;\hat{d}) (l \cos(ly))^2 \, dy \\
\hat{\gamma}_{33} =& \int_{-L}^{L} F(y;\hat{d}) (l \sin(ly))^2 \, dy
\end{aligned} \tag{51}$$

We remark that, strictly speaking, the domain of integration in the barotropic dissipation terms should be taken over $-L < y < L$. However, since the component of meridional boundary layer velocity due to the baroclinic flow in the troposphere decays rapidly away from the origin, we extend these integrals to infinity for simplicity and at the expense of a small error in the dissipation terms, as done elsewhere in MB.

Further simplification of the matrix $\hat{\Gamma}$ can be achieved by exploiting the symmetry of the zonal component of the baroclinic eigenfunction. In particular it is straightforward to show that

$$\begin{aligned}
&m = 1 \Rightarrow \hat{u} \text{ symmetric} \Rightarrow \hat{\gamma}_{13} = 0 \\
&m = 2 \Rightarrow \hat{u} \text{ antisymmetric} \Rightarrow \hat{\gamma}_{12} = 0.
\end{aligned} \tag{52}$$

### 3.2. Normal form rescaling

The amplitude equations for the dissipative equatorial baroclinic barotropic waves (41) can be recast in a normal form. Following MB, we define the rescaled amplitudes $\hat{A} = \sqrt{r_A} A$, $\hat{B}^S = s_B \sqrt{r_B} B^S$, $\hat{B}^A = s_B \sqrt{r_B} B^A$, the rescaled time $\hat{\tau} = \tau/\tau_0$ and zonal coordinate $\hat{x} = x/x_0$. Upon removing the hats the dissipative rescaled equatorial baroclinic

barotropic equations (DREBB) are

$$\begin{aligned} A_\tau - DA_{xxx} + (A\,B^S)_x &= -\,\bar{\Delta}(\gamma_{11}A + \gamma_{12}B^S + \gamma_{13}B^A) - \bar{d}_\theta\gamma_\theta A \\ B^S_\tau - B^S_{xxx} + AA_x &= -\,\bar{\Delta}(\gamma_{12}A + \gamma_{22}B^S) \\ B^A_\tau - B^A_{xxx} &= -\,\bar{\Delta}(\gamma_{13}A + \gamma_{33}B^A) \end{aligned} \tag{53}$$

The values of the rescaling coefficients are presented in the appendix to MB (2003)

$$\begin{aligned} (\sqrt{r_A}, \sqrt{r_B}, x_0, \tau_0, s_B) = (1.63, 2.33, 0.60, 1.96, 1) \quad \text{for } m = 1 \\ (1.72, 2.65, 0.55, 4.22, -1) \quad \text{for } m = 2. \end{aligned} \tag{54}$$

Using the boundary layer dissipation rate $\hat{d} = 0.67$ the values for the rescaled dissipation coefficients become

$$\begin{aligned} \gamma_\theta \equiv \frac{\hat{\gamma}_\theta\tau_0}{r_A} &= \begin{cases} 0.98 \\ 2.11 \end{cases} & \gamma_{11} \equiv \frac{\hat{\gamma}_{11}\tau_0}{r_A} &= \begin{cases} 0.29 \\ 1.05 \end{cases} \\ \gamma_{12} \equiv \frac{s_B\hat{\gamma}_{12}\tau_0}{\sqrt{r_A\,r_B}} &= \begin{cases} 0.29 \\ 0 \end{cases} & \gamma_{13} \equiv \frac{s_B\hat{\gamma}_{13}\tau_0}{\sqrt{r_A\,r_B}} &= \begin{cases} 0 \\ 1.11 \end{cases} \\ \gamma_{22} \equiv \frac{\hat{\gamma}_{22}\tau_0}{r_B} &= \begin{cases} 0.40 \\ 0.79 \end{cases} & \gamma_{33} \equiv \frac{\hat{\gamma}_{33}\tau_0}{r_B} &= \begin{cases} 0.50 \\ 1.01 \end{cases} \end{aligned} \tag{55}$$

where the first values correspond to $m = 1$ and the second values to $m = 2$.

The energy exchange properties of equations (53) have been studied by MB for the case when $\bar{\Delta} = \bar{d}_\theta = 0$. We remark that the energy is simply the integral of the amplitudes added in quadrature

$$E = \frac{1}{2}\int [A^2 + (B^S)^2 + (B^A)^2]\,dx \tag{56}$$

while each of the wave components of energy are

$$E_A = \frac{1}{2}\int (A')^2]\,dx, \tag{57}$$

where the wave components are defined implicitly by

$$A = \bar{A} + A' = \int A\,dx + A' \tag{58}$$

and similarly for $B^S$ and $B^A$. The effects of the dissipation terms will be elucidated in the coming sections when linear and non-linear solutions are studied. Note that, from equation (52) when $m = 1$, antisymmetric barotropic waves decouple from the other modes and simply disperse and decay. Conversely when $m = 2$ the dissipation does not couple the symmetric barotropic waves to the (antisymmetric) baroclinic waves. Their coupling occurs through the original, energy conservative terms on the right hand side. Dissipative coupling between the antisymmetric baroclinic waves and the antisymmetric barotropic waves does, however, occur when $m = 2$.

# 4. Linear Theory of the DREBB

For the purposes of discussion, we fix the values of the boundary thickness ratio $\bar{\Delta} = 2$ and, when considering thermal dissipation its rate shall be $\bar{d}_\theta = 0.67$ as discussed above equation (30).

## 4.1. Dissipation of zonal mean flows

Taking the zonal mean of the equations (53) we find the first novel feature of this model, that zonal mean flows evolve linearly through a nearly degenerate dissipation matrix. For $m = 1$ with no thermal dissipation the mean flow equations are

$$\begin{bmatrix} \bar{A}_\tau \\ \bar{B}^S_\tau \\ \bar{B}^A_\tau \end{bmatrix} = - \begin{bmatrix} 0.6 & 0.6 & 0 \\ 0.6 & 0.8 & 0 \\ 0 & 0 & 1 \end{bmatrix} \cdot \begin{bmatrix} \bar{A} \\ \bar{B}^S \\ \bar{B}^A \end{bmatrix}. \tag{59}$$

This matrix has eigenvalues

$$\lambda_1 = -0.09, \quad \lambda_2 = -1.31, \quad \lambda_3 = -1.0 \tag{60}$$

and recognizing that the rescaled time unit corresponds to 22 days we find decay times, $T_i = |\lambda_i^{-1}|$ of

$$T_1 = 244 \text{ days}, \quad T_2 = 17 \text{ days}, \quad T_3 = 22 \text{ days}. \tag{61}$$

The third eigenvalue clearly corresponds to a pure antisymmetric barotropic mode. The first two eigenvalues correspond to mixed symmetric barotropic and $m = 1$, symmetric baroclinic mean flows. The very long timescale associated with $T_1$ is a reflection of the nearly degenerate nature of the matrix. Therefore mean flows will relatively quickly decay to the eigenfunction associated with the smallest eigenvalue, $\lambda_1$, which we call the slow or slaved state. Since the timescale associated with the smallest eigenvector is well beyond the time at which other physical effects are expected to intervene, the boundary layer dissipation matrix behaves as though it were degenerate in the asymptotic equations. The mixed baroclinic/barotropic eigenfunction corresponding to $T_2$ is the most rapidly dissipated mean state and we will refer to it as the fast eigenfunction or adjustment flow.

The meridional structure of the mean zonal flow can be reconstructed using the eigenvectors for the slow and fast modes

$$\bar{B}^S \approx -0.85\bar{A}, \quad \bar{B}^S \approx 1.18\bar{A}, \tag{62}$$

respectively. The expression for the total mean zonal flow as a function of the rescaled amplitudes is

$$u = \frac{\bar{B}^S(\tau)}{\sqrt{r_B}} l \cos(l\, y) \pm \frac{\bar{A}(\tau)}{\sqrt{r_A}} e^{-y^2/2} \left[\frac{3}{2} - y^2\right] \tag{63}$$

where $l = \sqrt{3}$ and the positive and negative signs correspond to the bottom and the top of the free troposphere, respectively. The meridional structure of zonal flow at the top and bottom of the troposphere and the meridional and zonal component of the boundary layer flow are plotted in figures 2 and 3. Using a barotropic shear which attains a velocity of 3.7 $\mathrm{ms}^{-1}$ at the equator, figure 2 displays the slaved flow and figure 3 displays the adjustment flow.

Figure 2 (b) shows the zonal flow at the base of the troposphere for the slaved flow. Clearly in the slaved state there is only a weak zonal flow (about $-1\,\mathrm{ms}^{-1}$) at the base of the free troposphere near the equator. The meridional velocity in the boundary layer, figure 2 (c), never rises above 1 $\mathrm{ms}^{-1}$. In contrast, the zonal flow for the adjustment flow at the base of the troposphere near the equator is about 9 $\mathrm{ms}^{-1}$ in figure 3 (b). The meridional boundary layer flow is also much larger - about 4 $\mathrm{ms}^{-1}$ in figure 3 (c) - and of the opposite sign of its counterpart in figure 2. In both of these cases, the zonal flow in the boundary layer (figures 2 and 3 (d)) near the equator is large if the corresponding meridional flow is large. Similarly the zonal flow at the top of the troposphere near the equator (figures 2 and 3 (a) ) is large if its counterpart at the base of the troposphere is small. These results clearly reflect the physical principle that boundary layer dissipation tends to minimize the meridional (and thereby zonal) velocity in the boundary layer near the equator. Therefore, boundary layer dissipation tends to drive zonal mean flows to a minimum velocity at the base of the troposphere.

For $m = 2$ the zonal mean flows evolve according to

$$\begin{bmatrix} \bar{A}_\tau \\ \bar{B}^S_\tau \\ \bar{B}^A_\tau \end{bmatrix} = - \begin{bmatrix} 2.1 & 0 & 2.22 \\ 0 & 1.58 & 0 \\ 2.22 & 0 & 2.02 \end{bmatrix} \cdot \begin{bmatrix} \bar{A} \\ \bar{B}^S \\ \bar{B}^A \end{bmatrix}. \tag{64}$$

where, in this case, one unit of the long timescale corresponds to 46 days. The eigenvalues of the dissipation matrix are

$$\lambda_1 = 0.16, \quad \lambda_2 = -4.28, \quad \lambda_3 = -1.58 \tag{65}$$

so that the first eigenvalue now corresponds to a growing mode. The timescales associated with these eigenvalues are

$$T_1 = 288 \text{ days}, \quad T_2 = 11 \text{ days}, \quad T_3 = 29 \text{ days}. \tag{66}$$

In this case the third eigenvalue represents a decaying symmetric barotropic mean wind. The first eigenvalue yields a small growth of mixed antisymmetric barotropic and antisymmetric, $m = 2$ baroclinic mean flow. The fact that one mode grows does not pose significant problems for the theory as again, it happens on timescales much larger than those of physical interest. In this case, we would expect smaller scale barotropic and baroclinic modes to be spun up prior to the $T_1$ timescale since, as stated before equation

(46) a full description of the boundary layer dissipation would require a complete basis for the antisymmetric baroclinic and barotropic modes. Including only a few more baroclinic and barotropic modes actually destroys the positive eigenvalue, but since these modes do not resonate with the antisymmetric, $-10\,\mathrm{ms}^{-1}$ baroclinic wave and only interact linearly. Finally, the second mixed mode decays on timescales of 11 days and so we can expect a balanced mean flow state corresponding to the first eigenvector to prevail over long timescales.

Again the meridional structure of the mean zonal flow is reconstructed using the eigenvectors for the slow and fast modes

$$\bar{B}^A \approx -1.02\bar{A}, \quad \bar{B}^A \approx 0.98\bar{A}, \tag{67}$$

respectively. When $m = 2$ the total mean zonal flow is antisymmetric about the equator and is given by

$$u = \frac{\bar{B}^A(\tau)}{\sqrt{r_B}} l \sin(l\,y) \pm 2\sqrt{2}\,\frac{\bar{A}(\tau)}{\sqrt{r_A}} e^{-y^2/2}\left[y - \frac{y^3}{3}\right] \tag{68}$$

where $l = \sqrt{5}$ and the positive and negative signs correspond to the bottom and the top of the troposphere, respectively. The slaved zonal flow is plotted in figure 4 and the adjustment flow in figure 5. For the slaved flow, it is again clear that zonal flow is small at the bottom of the troposphere, especially near the equator. The meridional flow in the boundary layer is absolutely negligible in this case. Conversely, the adjustment flow has exceedingly strong zonal flow at the base of the troposphere and correspondingly strong flows in the boundary layer.

We conclude that the effect of the near degeneracy of the boundary layer dissipation matrix is to quickly drive mean zonal flows to a slow eigenfunction, the slaved mean flow state. The slaved state has minimal flow in the boundary layer and therefore a very weak wind at the base of the troposphere. Since the barotropic and baroclinic components of the velocity essentially cancel at the base of the troposphere, they are additive at the top of the troposphere. Therefore the slaved state has very strong winds at the top of the troposphere.

### 4.2. Breaking the degeneracy; the effect of thermal dissipation on mean flows

Increasing the thermal dissipation has the effect of breaking the near degeneracy due to pure boundary layer dissipation. Using $m = 1$ we calculate the eigenvalues and eigenvectors of the dissipation matrix as a function of $\hat{d}_\theta$. Figure 6 (a) shows the dissipation times for increasing $\hat{d}_\theta$ among a range of reasonable values. The timescale of the slow mode rapidly decreases from the 244 day time associated with purely boundary layer dissipation. Nonetheless, for all reasonable values, $\hat{d}_\theta < 0.67$ the slow timescale remains above 50 days, well separated from the fast timescale. The latter, in turn, is only moderately affected by thermal damping, remaining always on the order of 15 days.

In figure 6 (b) is plotted the ratio of the zonal velocities at the bottom of the troposphere at the equator for the eigenfunctions of the dissipation matrix as a function of $\hat{d}_\theta$. Clearly, even when $\hat{d}_\theta = 0$ the wind speed of the slow mode (the negative branch) does not vanish there; as we have discussed, the zonal velocity of the slow mode becomes low over a broad meridional range. Increasing thermal damping increases the barotropic contribution to the slow mode while decreasing its contribution to the fast mode.

### 4.3. Linear theory of dissipated waves for slaved mean flows

Since mean flows are not constant in time, the linear theory of barotropic and baroclinic waves in the presence of mean flows is not well defined. However, it is useful as a very relevant approximation to consider the linear theory of waves in the presence of slaved mean flows assuming that the mean velocities remain constant. We describe the linear theory for four cases of $m = 1$ waves interacting with mean shears which were chosen to reside in the slaved state. The first two cases have no thermal dissipation while the latter two cases use $\hat{d}_\theta = 0.67$; only the two examples with the most extreme behavior are shown in figures 7 and 8. The mean shears were chosen to have moderate values that can be expected from the climate record so the barotropic mean flow takes on both positive and negative values. Since the amplitude equations are valid only for the longest wavelengths in the domain we only consider linear theory for the first six zonal wavenumbers.

In case 1 the equatorial barotropic mean shear is 2.5 $\text{ms}^{-1}$ at the bottom of the troposphere so that the baroclinic mean shear is -3.6 $\text{ms}^{-1}$ there. The dissipation time as a function of integer zonal wavenumber is plotted in figure 7 (a). It is clear that the dissipation times for both the slow and fast modes remain well separated and do not change significantly over this range of wavenumbers. MB studied the effect of barotropic and baroclinic shears on the wave speeds and found that the mean shears could produce a significant change in wave speeds, on the order of 5 $\text{ms}^{-1}$. Plotted in figure 7 (b) are the wave speeds for case 1. The presence of boundary layer dissipation does not qualitatively alter the conclusions of the undamped theory. However, note that the mean flows impart a splitting of the two sets of waves, one of which is damped more rapidly than the other. In this case, the upper wave branch (waves moving westward more slowly) corresponds to the set of slow modes. We describe the linear theory of case 2 without a figure. In case 2 there is also no thermal dissipation and mean flows have the opposite sign of case 1; a barotropic mean shear of -2.5 $\text{ms}^{-1}$ and a baroclinic mean shear of 3.6 $\text{ms}^{-1}$. In this case, though the fast mode damps at about 17 days the slow mode timescale drops from 244 days to less than 100 days over the first six wavenumbers. Again the wave speeds are not significantly altered, however the slowly damped waves travel westward with greater velocity.

Cases 3 and 4 have $\hat{d}_\theta = 0.67$. In case 3 (not plotted) the mean zonal barotropic shear is 2.5 $\text{ms}^{-1}$ making the baroclinic wind -3 $\text{ms}^{-1}$. The damping time for the fast and slow

modes do not change significantly with wavenumber, the former being about 15 days and the latter about 60 days. The wave speeds have the same qualitative behavior as in the non-dissipated case and again the weakly damped waves travel westward more slowly than the strongly damped waves. Case 4 uses a mean barotropic shear of -2.5 $ms^{-1}$ so that the baroclinic shear is 3 $ms^{-1}$. Figure 8 (a) shows that the slow modes do not remain well separated from the fast modes, both having a timescale of approximately 25 days at wavenumber six. Clearly the designations "slow" and "fast" are no longer valid. The wave speeds are qualitatively the same as the earlier cases with the slow branch traveling westward with greater velocity.

In conclusion the linear theory of dissipated baroclinic barotropic waves exhibits a myriad of different behaviors. The general features of the wave speeds appear to be unaffected by dissipation. When there is no thermal dissipation one set of waves is rapidly damped while the other remains slowly damped for all of the asymptotically valid wavenumbers. However, for significant amounts of thermal dissipation the two branches do not remain well separated, both rapidly decaying.

## 5. Numerical simulations of the amplitude equations in the presence of dissipation

We integrate equations (53) over a zonal domain which corresponds to the circumference of the Earth. The numerical integrations reported here were performed using a de-aliased pseudo-spectral method with at least 64 modes of spatial resolution combined with a fourth order Runge-Kutta time discretization. For the simulations describing solitary waves, we used 256 modes of resolution. Conservation of energy to within $10^{-6}$ is satisfied for all numerical solutions and as in MB, we ensured that less than 4% of the energy resided in modes higher than $k = 8$ for all times in order to be consistent with the long wavelength asymptotics. In order to reconstruct the velocity fields the standard value of $c = 50$ $ms^{-1}$ and the choice $\epsilon = 0.1$ is used.

With regard to the plots, the waves in all of the flow vector figures are shown in the carrier wave frame of reference, $-16.6\,ms^{-1}$. Furthermore, the velocity vectors in the troposphere are plotted for the same example at all times using the same scale; both of the solitary waves use the same scales. The vectors in the boundary layer are stretched in order to highlight the flow features, but also use the same scales for a given example.

In this section we consider four examples of dissipative equatorial baroclinic and barotropic waves in the case $m = 1$. This corresponds to a symmetric baroclinic wave and mean flow interacting with barotropic waves. The antisymmetric barotropic waves evolve under linear dispersion and dissipation in this situation and, since they have no effect on the other waves or mean flows, we always consider zero initial data for these waves. Therefore the setting is symmetric barotropic and baroclinic mean shears in the presence

of symmetric barotropic and equatorial baroclinic waves. First we consider the effect of boundary layer dissipation on solitary waves which arise in the ideal setting using , $\bar{\Delta} = 2$ and $\bar{d_\theta} = 0$. We then revisit two examples considered by MB in the ideal context and consider the evolution of the same initial conditions in the presence of both boundary layer and thermal dissipation; $\bar{\Delta} = 2$ and $\bar{d_\theta} = 0.67$. The second example was chosen in order to study the exchange of energy from equatorial barotropic Rossby waves with significant midlatitude projection to equatorial baroclinic Rossby waves which are concentrated around the tropics. The third example considers the transfer of energy from the tropical equatorial baroclinic waves to the barotropic waves with significant midlatitude projection. By comparing the ideal results in MB with those in the presence of boundary layer drag and thermal dissipation, we can see the effects of dissipation on the rate and amount of energy exchange between the tropical and extra-tropical waves that were discussed in MB. In the final example, we again only use boundary layer dissipation and begin with a mean flow which is already in a slaved state. Using random initial wave data we consider the long time evolution of the waves and we shall find that they evolve to a slaved state of their own with extremely interesting patterns.

### 5.1. Effect of boundary layer dissipation on Solitary waves

Biello and Majda (2003) construct solitary wave solutions of the undamped amplitude equations (53) of the form

$$\begin{aligned} A(x-ct) =& a\ \mathrm{sech}^2\left(\frac{x-ct}{\lambda}\right) + \bar{A} \\ B^S(x-ct) =& -b\ \mathrm{sech}^2\left(\frac{x-ct}{\lambda}\right) + \bar{B}. \end{aligned} \tag{69}$$

Such exact solutions are archetypes of more general localized structures and provide an idealized setting where the effects mean shear and non-linear advection could be studied. We now add the effect of boundary layer dissipation on such localized waves. In the setting without dissipation, to every solitary wave there corresponds another through interchanging $A \to -A$. This is a reflection of the vertical symmetry of the undamped equations which we expect boundary layer dissipation to break. The non-zero constants, $\bar{A}$, $\bar{B}$ give solitary waves in specific baroclinic and barotropic mean shears.

We numerically integrate two solitary wave solutions for 20 days using $\bar{\Delta} = 2$ and $d_\theta = 0$ and compare the results to the initial waves. The waves have wave amplitudes which are comparable to the mean wind and shears. The initial condition of the first wave is shown in figure 9; a 11400 km wave traveling at $-15\,\mathrm{ms}^{-1}$ in a barotropic mean wind of $3\,\mathrm{ms}^{-1}$ and a baroclinic mean shear of $-5\,\mathrm{ms}^{-1}$. This soliton in a shear flow has a cyclonic equatorial baroclinic component and an anti-cyclonic barotropic component. The relation of $A$ and $B^S$ is reasonably near that for the slow slaved state in equation (62) so we expect

boundary layer dissipation to be inefficient here. The winds are much stronger in the top of the troposphere, $8\,\mathrm{ms}^{-1}$ (figure 9 (c)), compared with $-2\,\mathrm{ms}^{-1}$ (figure 9 (b)) at the base. The boundary layer flow converges at the equator except at the soliton where it is divergent and westerly. Notice that the solitary wave itself has the effect of locally reversing the mean flow in the troposphere. After 20 days the wave is shown in figure 10. Clearly very little dissipation has taken place, the wave having simply traveled eastward in the moving frame.

The initial condition for second solitary wave in figure 11 reverses the sign of the baroclinic flow component of the previous wave so that both components are anti-cyclones. Here there is a strong projection on the fast component in equation (62) so we expect the dissipation to be very efficient. In this instance there is an $8\,\mathrm{ms}^{-1}$ mean wind at the base of the troposphere and a correspondingly large boundary layer flow which diverges from the equator everywhere except in the solitary wave. Again the wind at the center of the solitary wave is in the opposite direction of the mean wind and attains a maximum easterly wind speed of $7\,\mathrm{ms}^{-1}$ at the base of the troposphere. As a result of the vertical baroclinic symmetry, in the absence of dissipation this solution would behave exactly like the previous solution. Figure 12 shows that after only 10 days the solitary wave is barely recognizable having dissipated to about half its strength. Its ghost remains in the persistent boundary layer flow which continues to dissipate the wave.

We conclude that many of the solitary waves present in the ideal case can be expected to persist in the presence of boundary layer dissipation. In particular, localized structures which are superimposed on slaved or nearly slaved mean flows and which have the necessary weak flow at the base of the troposphere can exist quite unaffected by dissipation over intraseasonal timescales. Specifically superimposed cyclonic (anti-cyclonic) barotropic and anti-cyclonic (cyclonic) baroclinic solitary waves will be long lived even in the presence of boundary layer dissipation. Solitary waves with the same sense of barotropic and baroclinic rotation will tend to dissipate rapidly.

### 5.2. Effect of dissipation on tropical winds forced by midlatitude waves

MB consider an initial condition with baroclinic wave amplitude equal to zero. The energy is concentrated in the barotropic wave train and the baroclinic and barotropic mean flows. There is no barotropic zonal mean shear whereas the baroclinic mean shear velocity is $5\,\mathrm{ms}^{-1}$ at the equator. Using the same initial conditions MB discussed how vertical mean shear arising from baroclinic mean shear provides a route for midlatitude connections. The initial condition is shown in figure 13 (a) and the corresponding flow field at the bottom and top of the troposphere are shown respectively in figures 13 (c) and (d). The boundary layer flow, which is absent in the ideal case, is shown in figure 13 (b). It consists of three strong eastward divergent winds at the flow maxima at the base of the troposphere, which are also the maxima of the barotropic waves. There also westward and eastward flows at

higher latitudes. These are located at the maxima and minima of the barotropic waves and are a reflection of the strong winds at midlatitudes associated with the barotropic waves.

After 14 days much dissipation has occurred but there has also been a significant transfer of energy to baroclinic waves. In figure 14 strong baroclinic wave activity is evident in the left half of the domain. The dominance of the baroclinic component of the velocity field around $x = 15$ is the remnant of the "westerly wind burst-like" event that was described by MB. Furthermore, it is clear from the boundary layer flow, figure 14 (b), that the dissipation is concentrated around this structure.

As a measure of the effect of dissipation we compare the diagnostics of the ideal case considered by MB at 14 days to those of the dissipative case considered here. In particular the baroclinic mean shear decreases from $5\,\mathrm{ms}^{-1}$ in the ideal case to $2.5\,\mathrm{ms}^{-1}$ in the presence of dissipation. There is actually barotropic mean shear generation in this example with the mean shear decreasing from zero to $-0.75\,\mathrm{ms}^{-1}$, consistent with its drive to a slaved mean flow state. For the energy diagnostics we define $\chi_D$ to be the ratio of energies at 14 days in the dissipative example to that in the ideal example. $D$ denotes the energy considered and shall take the values $D = tot, A, B$ which are the total energy, baroclinic wave energy and barotropic wave energy, respectively. The numerical results yield

$$\chi_{tot} = 0.36, \quad \chi_A = 0.22, \quad \chi_B = 0.62 \tag{70}$$

Clearly the dissipation is effective at inhibiting baroclinic wave forcing by barotropic waves. However as is evident from figure 14, the most interesting strong localized structures do persist. After 14 days, the ratio of baroclinic to barotropic wave energies in the ideal case was 1.1 indicating a strong connection whereas in the dissipative setting the connection is much weaker with the ratio being 0.4.

### 5.3. Effect of dissipation on midlatitude waves driven by tropical winds

MB considers the transfer of energy from an initial equatorial baroclinic wave train to barotropic waves with significant midlatitude projection. Using a baroclinic initial mean shear of $5.0\,\mathrm{ms}^{-1}$, a barotropic initial mean shear of $2.5\,\mathrm{ms}^{-1}$ and the same initial conditions of MB, the equations are numerically integrated in the presence of both boundary layer and thermal dissipation. The initial condition is shown in figure 15 (a), the baroclinic wave and mean amplitude being the dashed curve while the barotropic wave and mean amplitude is solid. The tropospheric flow associated with this wave train (figures 15 (c) and (d)) is highly antisymmetric between the top and bottom. The flow mainly consists of two localized baroclinic structures which are westerly at the ground plus an easterly wind leading located near $x = 35$. The boundary layer flow in figure 15 (b) is dominated by the two divergent, westerlies associated with the baroclinic cyclones in the troposphere. The easterly, convergent boundary layer flow associated with the easterly wind at the base of

the troposphere is weaker than its westerly counterparts. The boundary layer flow at higher latitudes is much weaker than the previous example since the barotropic amplitudes are much smaller here.

Figure 16 shows the amplitudes and flow fields after 14 days. Though the baroclinic waves are much dissipated, there is yet a significant transfer of energy to the barotropic waves in the form of the strong barotropic wave packet around $x = 15$. Nonetheless the strongest boundary layer winds occur near this packet and are divergent westerlies at the equator with easterly return flows at higher latitudes; indicative of the overlying barotropic wave.

In this example, the dissipative dynamics dramatically reduces the mean flows. At 14 days the baroclinic mean shear is $1.75\,\mathrm{ms}^{-1}$ while the barotropic mean shear is $0.71\,\mathrm{ms}^{-1}$. The ratio of the dissipated energies to the original energies are

$$\chi_{tot} = 0.24, \quad \chi_A = 0.13, \quad \chi_B = 0.29. \tag{71}$$

The energy of the dissipative waves is greatly reduced even in comparison to the previous example. As a measure of the efficacy of wave energy exchange, the ratio of barotropic to baroclinic wave energy in the non-dissipative case is 0.53 whereas in the dissipative case the ratio is 0.59. Since the two ratios are nearly equal it seems that dissipation does not greatly affect wave energy transfer in this example.

In summary, it appears that dissipation is very effective at modifying the mean flow of the waves which, in turn, can affect the energy transfer. Nonetheless coherent structures which exist in the non-dissipative examples persist in the dissipative examples. The basic qualitative result that there is significant energy exchange between the midlatitudes and the tropics in the presence of baroclinic mean shears is not affected by the dissipation.

### 5.4. Dissipation Balanced states

Since the previous examples suggest that the modification of the mean flows is the primary effect of dissipation on barotropic and baroclinic wave energy exchange, it is useful to consider initial mean shear profiles which do not change significantly under dissipation. In this section we consider the reduced equations for equatorial baroclinic and barotropic waves only in the presence of boundary layer dissipation; thermal dissipation is set to zero. We select initial conditions so that the mean flows are already slaved according to equation (62), the baroclinic mean shear is $-4.5\,\mathrm{ms}^{-1}$ at the base of the troposphere while the barotropic mean shear is $3.1\,\mathrm{ms}^{-1}$ at the base of the troposphere. The barotropic and baroclinic waves are initialized with random wave packets and the initial conditions, waves and means, are shown in figure 17 (a). The wind profile shows very strong barotropic waves near $x = 5$ and 25 while there is a mixed barotropic/ baroclinic packet near $x = 32$. The boundary layer flow in figure 17 (c) has a bit of everything. There are convergent easterly

and divergent westerly flows near the equator when there are strong winds in the overlying troposphere. Furthermore there are easterly flows at higher latitudes over regions where the tropospheric waves are strongly barotropic.

These initial conditions are integrated for long times compared to the other results we have presented. After 60 days of interaction the waves settle into a slowly decaying state (shown in figure 18) which persists for much later times. At this time the zonal mean baroclinic shear is $-3.5\,\mathrm{ms}^{-1}$ and the barotropic mean shear is $2.4\,\mathrm{ms}^{-1}$, having changed little from their initial conditions. The amplitudes in figure 18 (a) bear a striking resemblance to a packet of multiple slaved solitary waves of the type shown in figure 9. In fact, all of the wave packets travel at almost the same velocity, $-11\,\mathrm{ms}^{-1}$ with respect to the stationary frame. The barotropic amplitude has a clear plateau level with three localized wave packets at $x = 11, 20$ and 33 which oppose the mean barotropic shear. Similarly the baroclinic amplitudes have a clear plateau of the opposite sign of the barotropic plateau with three wave packets at the same location of the barotropic packets and which also oppose the baroclinic mean shear. The velocity field is extremely weak at the bottom of the troposphere being most dominant in the parts of the domain described as the plateau, in particular around $x = 5$ and 26. The boundary layer velocity is easterly and convergent in the regions where the dissipation is greatest.

At the top of the troposphere in figure 18 (d) the flow is again reminiscent of figure 9 (d). The centers of these solitary wave-like packets are anticyclonic vortices at the top of the troposphere. In the domains of the amplitude plateaus there are strong westerly winds at the equator which, when the plateau encounters a wave packet, turn around into long cyclonic gyres.

To summarize, random initial wave packets superposed on slaved mean flows have a tendency to settle into a collection of solitary wave-like packets over a slowly decaying mean flow state.

## 6. Concluding Discussion

We have derived a reduced model for the interaction of equatorial baroclinic and barotropic waves in the presence of boundary layer and thermal dissipation. The equations arise through the same long wave, low Froude number scaling of MB. The ratio of meridional to zonal flows in the troposphere is proportional to the small ratio of meridional length scales to zonal length scales. Conversely, the dominant balance in the atmospheric boundary layer allows meridional flows to be of the same order as zonal flows there. The lowest order asymptotics of the boundary layer are simply the equatorial Ekman equations. Therefore meridional and zonal boundary layer flows are proportional to the negative of the meridional pressure gradient in the overlying free troposphere. Equatorial high pressures at the base of the free troposphere drive divergent easterly flows in the boundary layer, enhancing

momentum dissipation. Similarly, low pressure centers at the bottom of the troposphere drive convergent easterly flows in the boundary layer, also a source of dissipation. When coupled to the equatorial baroclinic and barotropic long wave equations the lowest order source of boundary layer dissipation arises from the meridional component of the boundary layer flow. Therefore the dynamics drive the boundary layer flow to a minimum meridional velocity. This implies that the dynamics in the troposphere tends to minimize the pressure at the base or equivalently minimize the zonal velocity there. When incorporated into the amplitude equations (DREBB), this tendency is manifested as a near degeneracy of the boundary layer dissipation matrix. The presence of thermal dissipation breaks this degeneracy.

The results of numerical simulations indicate that boundary layer and thermal dissipation can significantly reduce the zonal mean flows unless they are initialized with small zonal velocity at the base of the free troposphere. The dissipation of mean flows, in turn, can inhibit wave energy exchange between the tropics and midlatitudes. In general the boundary layer dissipation is very efficient for barotropic/baroclinic cyclones or anti-cyclones but is much weaker for barotropic and baroclinic waves of opposite rotation. Strong coherent structures which form are less effected by the dissipation of mean flows since their energy transfer tends to be through direct wave-wave interaction, not mediated by baroclinic zonal mean flows. Initial wave trains interacting in the presence of balanced zonal mean climate states themselves evolve to a slaved wave state and persist over seasonal timescales. The dissipative balanced state consists of a collection of coherent wave packets similar to solitary waves for which the flow at the base of the free troposphere is minimum.

The systematic inclusion of boundary layer forcing can be applied to other asymptotic regimes. For example, Majda and Klein (2002) have derived scalings from the planetary to the synoptic scales in which there are resonant midlatitude to tropics connections. They can also be included in a straightforward manner in the more general theory equatorial Rossby waves in mean shears derived by Biello and Majda (2003). Finally, the unforced waves we have considered always decayed with time. However, the atmosphere is subject to seasonally varying thermal and convective forcing which, in the presence of damping could force the waves and mean flows into new balanced states. The inclusion of this seasonal forcing would provide an important extension of the theory which we shall consider in future work. Another interesting direction is to utilize these models for the equatorial ocean in a different parameter regime.

## Acknowledgments

We would like to thank our referees for a careful reading of the manuscript and their useful suggestions. The research of A.J. Majda is partially supported by NSF grant # DMS-9972865, ONR grant # N0014-96-1-0043 and NSF DMS-0139918. The research of

J.A. Biello was supported by an NSF VIGRE Postdoctoral Fellowship, # DMS-0083646 at RPI.

## REFERENCES

Biello, J. A. and A. Majda, "The Effect of Meridional and Vertical Shear on the Interaction of Equatorial Baroclinic and Barotropic Rossby Waves" *Studies in App. Math* (in press).

Boyd, J. R., "Equatorial solitary waves. Part I: Rossby Solitons" *J. Phys. Oceanogr.*, **10**, 1699-1717 (1980).

Heckley, W. A. and A. E. Gill, "Some simple solutions to the problem of forced equatorial long waves" *Quart J. Roy. Meteor. Soc.*, **110**. 203-217 (1984).

Hoskins, B.J. and F.-F. Jin, "The initial value problem for tropical perturbations to a baroclinic atmosphere" *Quart J. Roy. Meteor. Soc.*, **117**. 299-317 (1991).

Hoskins, B.J. and G.-Y. Yang, "The equatorial response to higher latitude forcing" *J, Atmos. Sci.*, **57**, 1197-1213 (2000).

Kasahara, A. and P.L. Silva Dias, "Response of planetary waves to stationary tropical heating in a global atmosphere with meridional and vertical shear" *J. Atmos. Sci*, **43**, 1893-1911 (1986).

Kiladis, G. and M. Wheeler, "Horizontal and vertical structure of observed tropospheric equatorial Rossby waves" *J. Geophys. Res.*, **100**, 22981-22997 (1995).

Lim, H. and C. P. Chang, "A theory for midlatitude forcing of tropical motions during winter monsoons" *J. Atmos. Sci.*, **39**, 2377-2392 (1981).

Lim, H. and C. P. Chang, "Generation of internal and external mode motions from internal heating: Effects of vertical shear and damping" *J. Atmos. Sci.*, **43**, 948-957 (1986).

Longuet-Higgins, M.S., "The eigenfunctions of Laplace's tidal equations over a sphere" *Proc. R. Soc. London, Ser. A.* , **262**, 511-607 (1968).

Majda, A. and M. Shefter, "Models for stratiform instability and convectively coupled waves" *J. Atmos. Sci.*, **58**, 1567-1584 (2001).

Majda, A. and R. Klein, "Systematic multi-scale models for the tropics" *J. Atmos. Sci.*, **60**, 357-372 (2003).

Majda, A., *Introduction to PDE's and Waves for the Atmosphere and Ocean*, American Mathematical Society, (2003).

Majda, A. and J.A. Biello, "The Nonlinear Interaction of Barotropic and Equatorial Baroclinic Rossby Waves" *J. Atmos. Sci* **60**, 1809-1821 (2003).

Moskowitz, B.M. and C.S. Bretherton: "An analysis of frictional feedback on a moist equatorial Kelvin mode" *J. Atmos. Sci.*, **57**, 2188-2206 (2000).

Neelin, J.D., "A simple model for surface stress and low-level flow in the tropical atmosphere driven by prescribed heating" *Q. J. Roy. Meteor. Soc.*, **114**, 747-770 (1988).

Neelin, J. D. and N. Zeng, "A quasi-equilibrium tropical circulation model - Formulation" *J. Atmos. Sci.*, **57**, 1741-1766 (2000).

Patoine, A. and T. Warn, "The interaction of long quasi-stationary waves with topography" *J. Atmos. Sci.*, **39**, 1018-1025 (1982).

Ripa, P., "On improving a one-layer oceal model with thermodynamics" *J. Fluid Mech.*, **303**, 169-201 (1995).

Wang, B. and T. Li, "A simple tropical atmosphere model of relevance to short-term climate variations" *J. Atmos. Sci.*, **50**, 260-284 (1993).

Wang, B. and X. Xie, "Low frequency equatorial waves in vertically sheared zonal flow" *J. Atmos. Sci.*, **53**, 449-467 (1996).

Webster, P. J., "Response of the tropical atmosphere to local steady forcing" *Mon. Wea. Rev.*, **100**, 518-541 (1972).

Webster, P. J., "Mechanisms determining the atmosphere response to sea surface temperature anomalies" *J. Atmos. Sci.*, **38**, 554-571 (1981).

Webster, P. J., "Seasonality in the local and remote atmospheric response to sea surface temperature anomalies" *J. Atmos. Sci.*, **39**, 41-52 (1982).

Wheeler, M., G.N. Kiladis and P. Webster, "Large scale dynamical fields associated with convectively coupled equatorial waves" *J. Atmos. Sci.*, **57**, 613-640 (2000).

Yanai M., B. Chen and W.W. Tung, "The Madden-Julian oscillation observed during the TOGA COARE IOP: Global view" *J. Atmos. Sci.*, **57**, 2374-2396 (2000).

This manuscript was prepared with the AAS LaTeX macros v5.0.

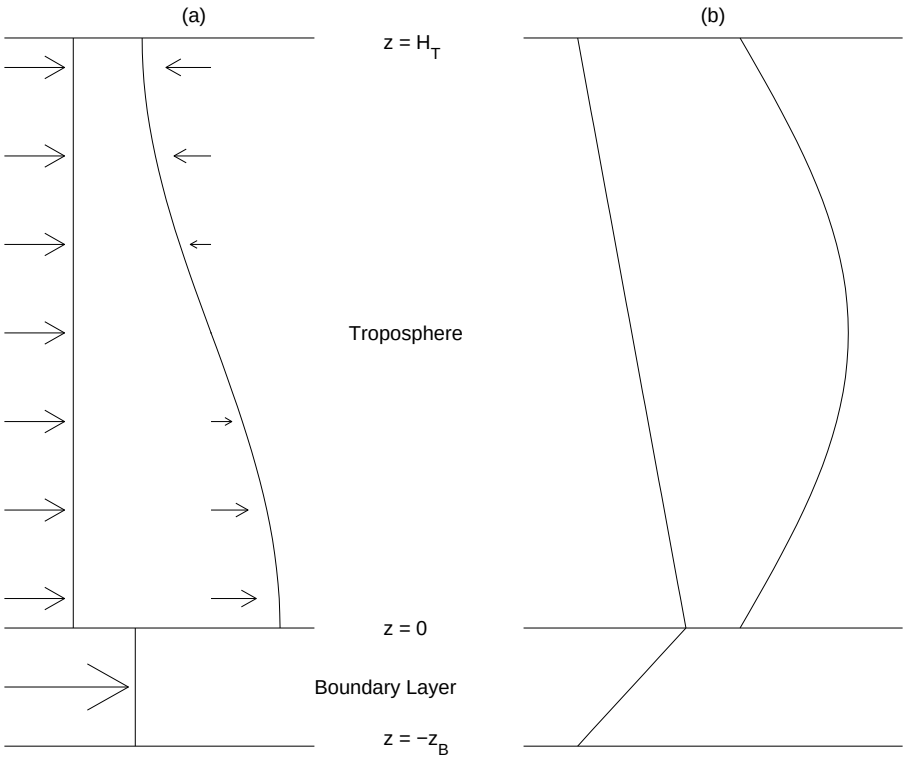


Fig. 1.— The structure of the velocity as a function of depth. (a) The left curve shows the barotropic mean wind in the free troposphere and boundary layer as a function of height; horizontal velocity is not continuous across $z = 0$ and thee is a vortex sheet there. The right curve shows the baroclinic mean shear which exists only in the free troposphere in this model. The dependence of the vertical velocity on height is shown in (b). In the left curve is plotted the the barotropic component which is zero at the ground, increases linearly to the top of the boundary layer and then decreases linearly to zero throughout the troposphere. This vertical velocity is the source of the divergence of the horizontal component of the barotropic flow in the troposphere. The baroclinic component is plotted at the right and is zero at the top and bottom of the free troposphere.

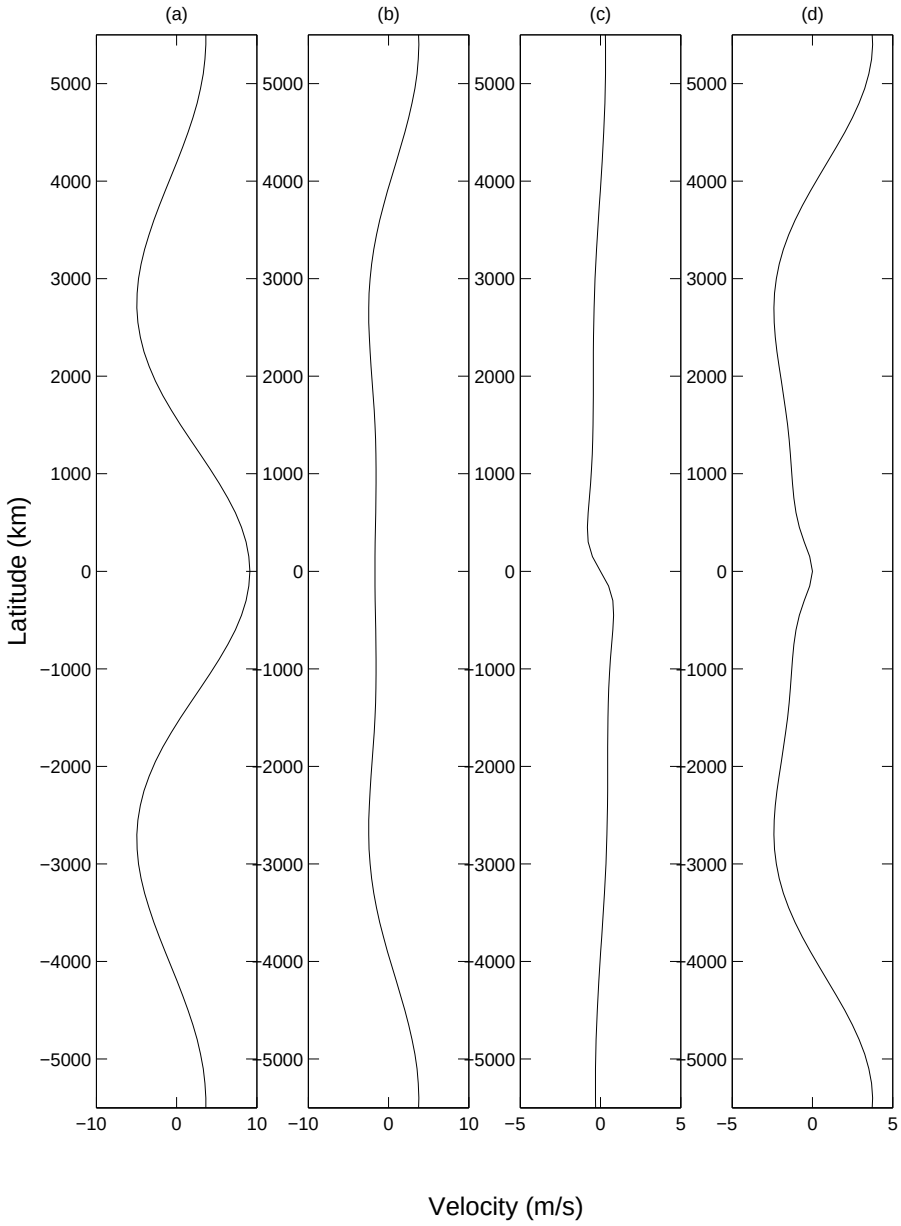


Fig. 2.— Zonal mean velocity fields for slaved flows, $m = 1$. (a) Zonal mean velocity at the top of the free troposphere. (b) Zonal mean velocity at the base of the free troposphere. (c) Meridional velocity in the boundary layer. (d) Zonal velocity in the boundary layer.

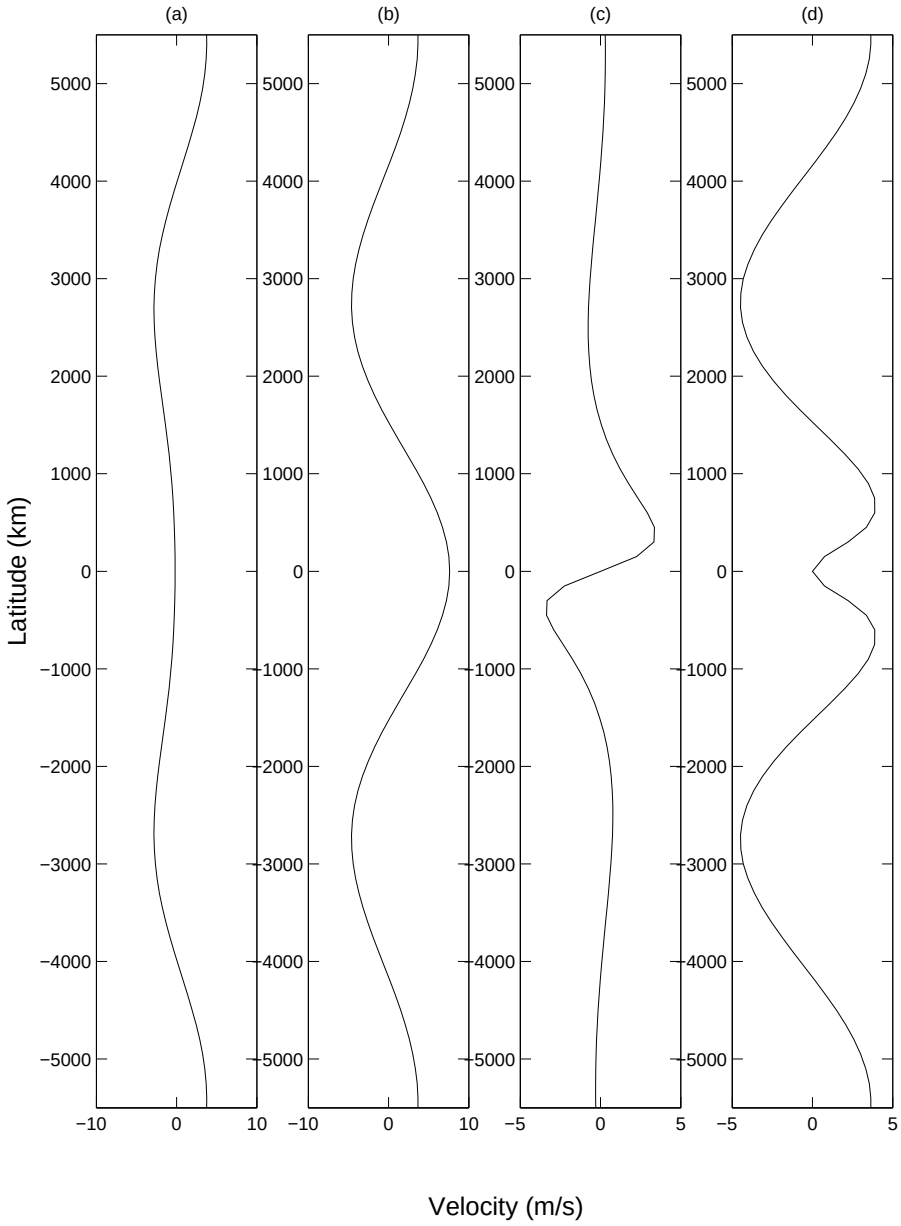


Fig. 3.— Zonal mean velocity fields for the adjustment flow, $m = 1$. (a) Zonal mean velocity at the top of the free troposphere. (b) Zonal mean velocity at the base of the free troposphere. (c) Meridional velocity in the boundary layer. (d) Zonal velocity in the boundary layer.

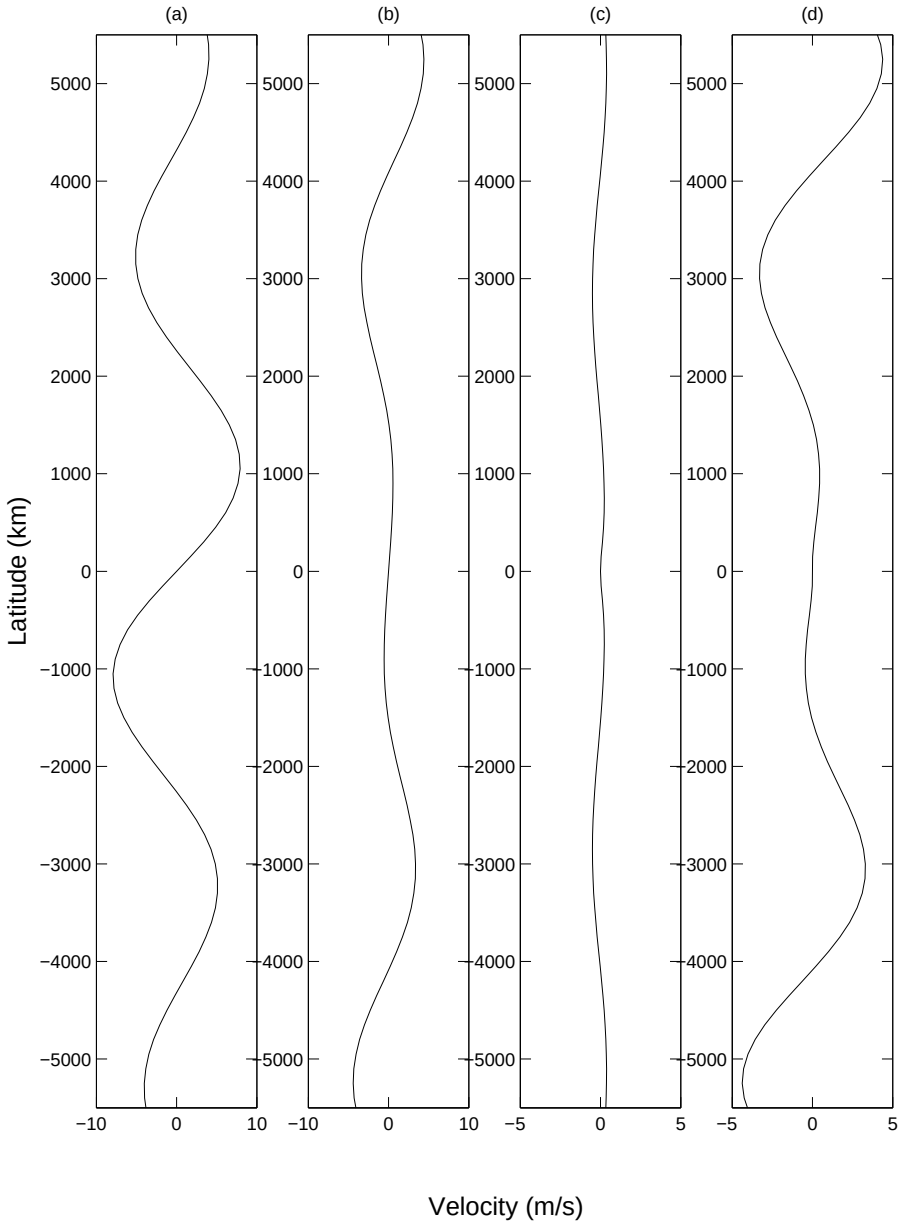


Fig. 4.— Zonal mean velocity fields for the slaved flow, $m = 2$. (a) Zonal mean velocity at the top of the free troposphere. (b) Zonal mean velocity at the base of the free troposphere. (c) Meridional velocity in the boundary layer. (d) Zonal velocity in the boundary layer.

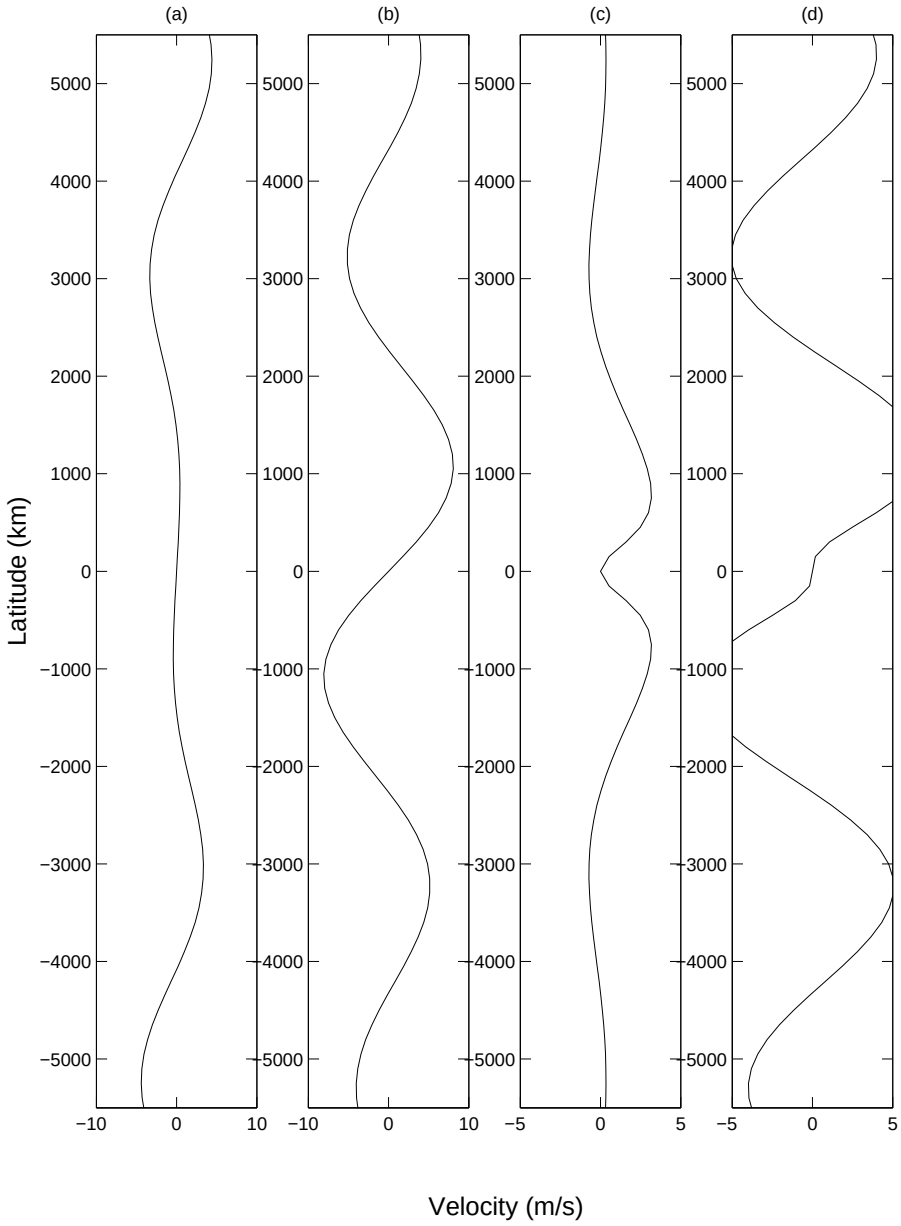


Fig. 5.— Zonal mean velocity fields for the adjustment flow, $m = 2$. (a) Zonal mean velocity at the top of the free troposphere. (b) Zonal mean velocity at the base of the free troposphere. (c) Meridional velocity in the boundary layer. (d) Zonal velocity in the boundary layer.

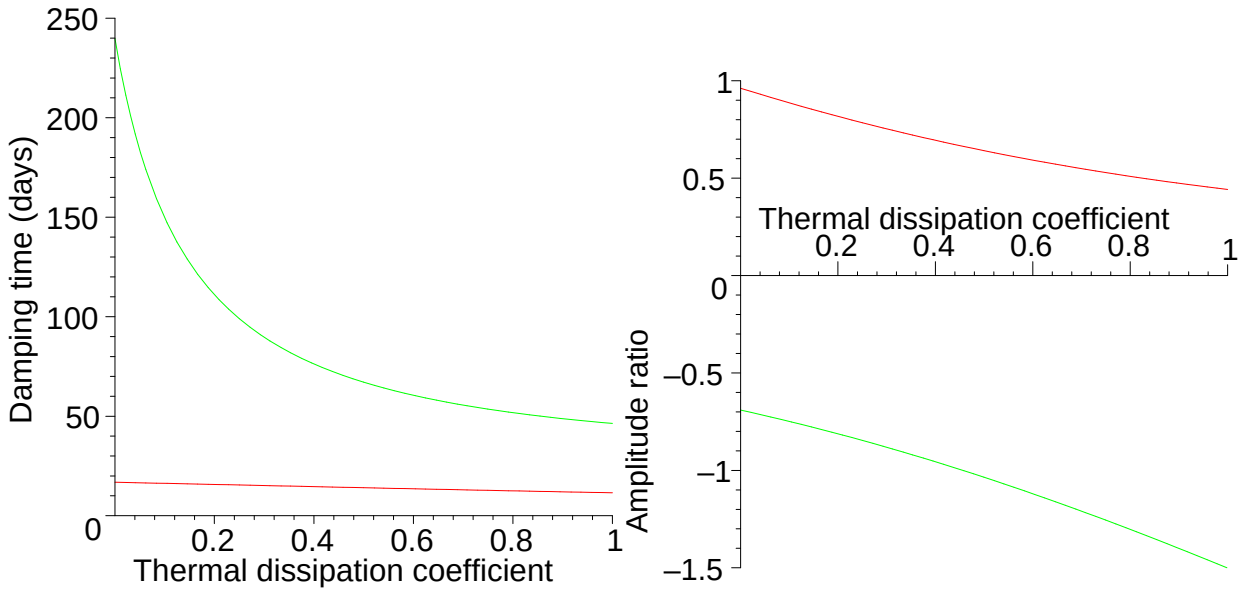


Fig. 6.— (a) Damping times as a function of thermal dissipation coefficient, $\hat{d}_\theta$ for $m = 1$. As $\hat{d}_\theta$ increases the timescale of the slow mode decreases dramatically, thereby destroying the exact slaving. However, the two decay timescales do remain well separated. The fast mode is essentially unaffected. (b) The ratio of the zonal mean barotropic to baroclinic velocity at the bottom of the free troposphere at the equator for each of the eigenvectors of the dissipation matrix. The negative branch corresponds to the slowly damped mode.

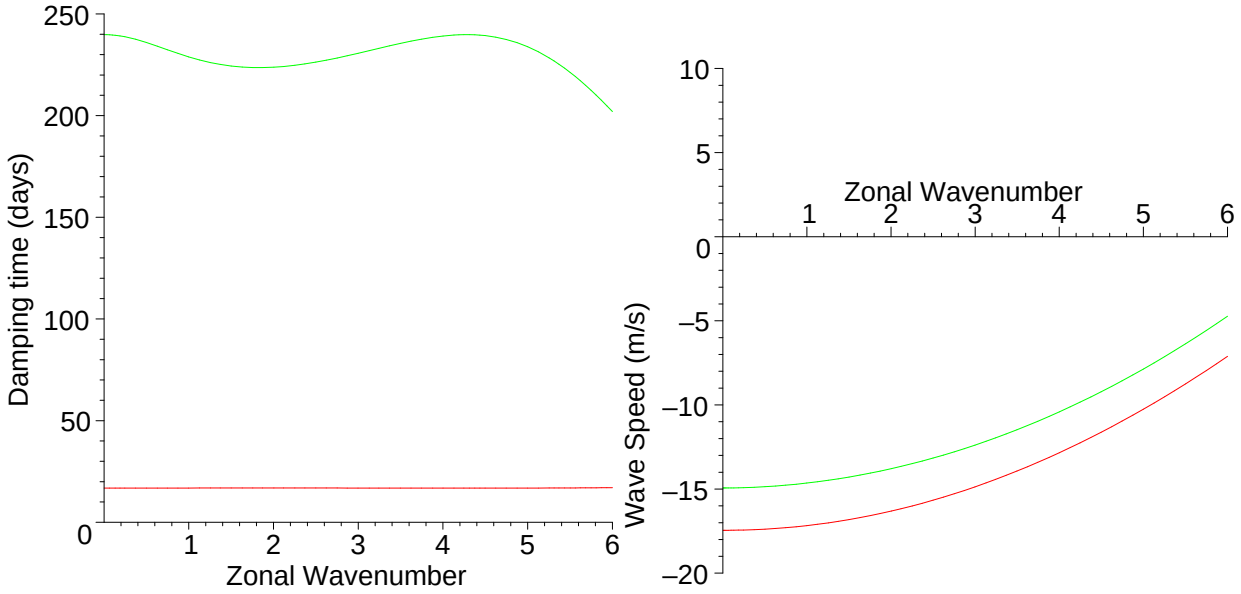


Fig. 7.— Case 1, $\hat{d}_\theta = 0$, positive barotropic wind at the base of the free troposphere at the equator. (a) Damping time as a function of zonal wave number. (b) Wave speed in the stationary frame as a function of zonal wavenumber. The upper branch corresponds to the slowly damped waves.

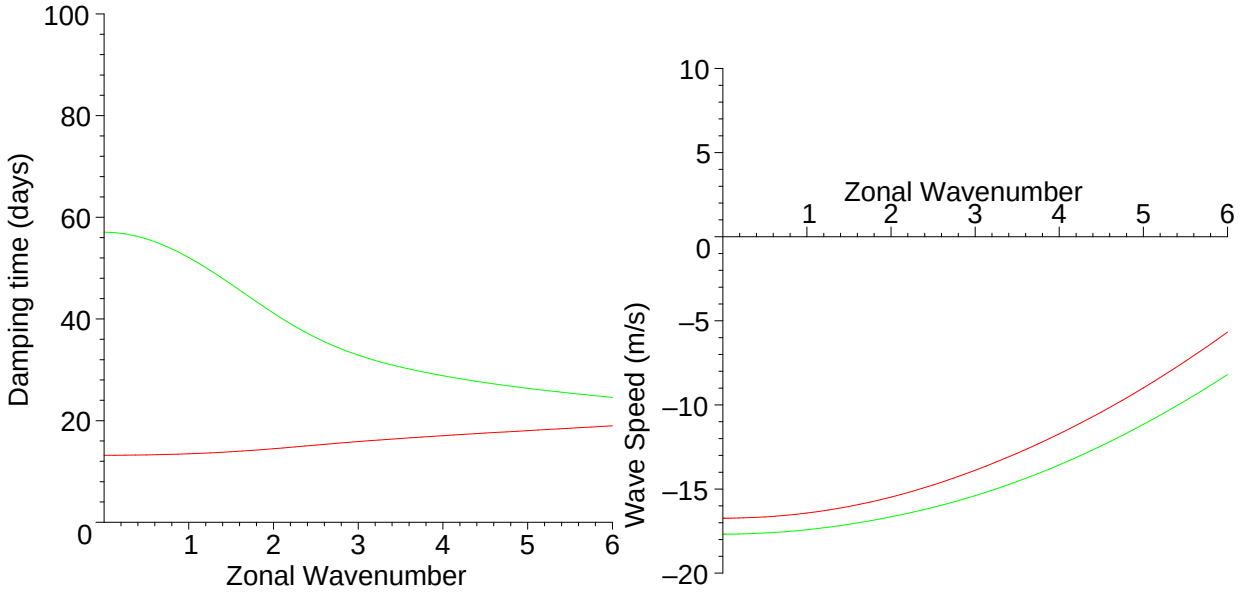


Fig. 8.— Case 4, $\hat{d}_\theta = 0.67$, negative barotropic wind at the base of the free troposphere at the equator. (a) Damping time as a function of zonal wave number. (b) Wave speed in the stationary frame as a function of zonal wavenumber. The lower branch corresponds to the more slowly damped waves.

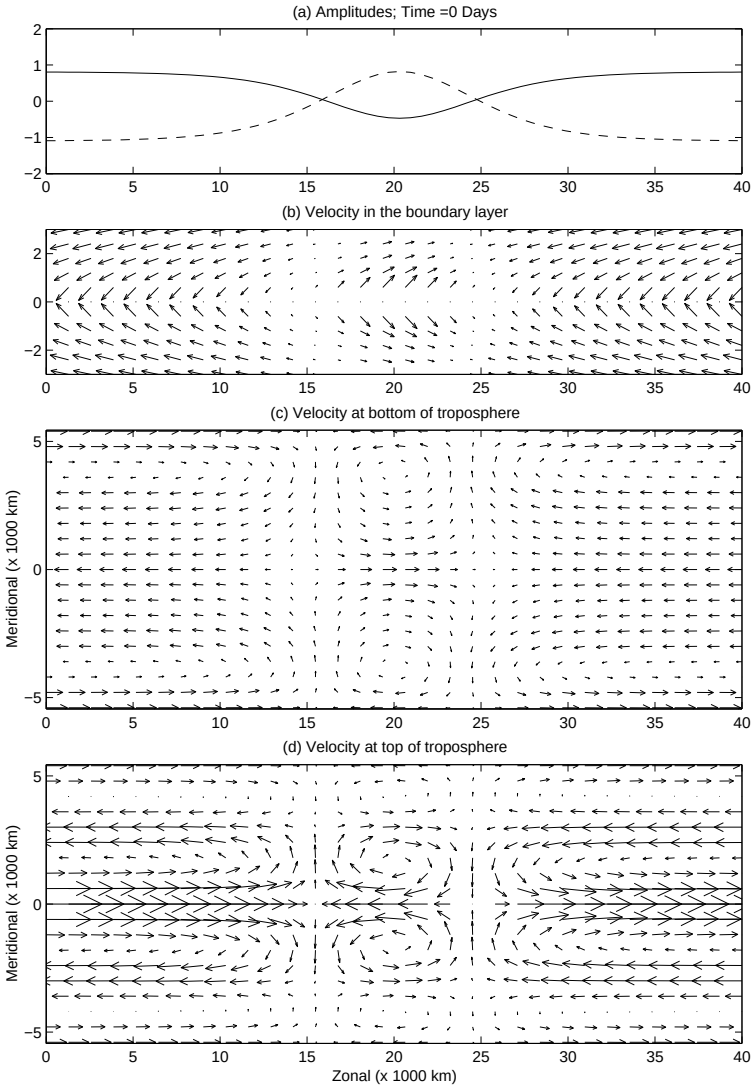


Fig. 9.— Initial condition for a 11400 km solitary wave traveling at $-15\,\mathrm{ms}^{-1}$. (a) Wave Amplitudes, solid - barotropic, dashed - baroclinic. (b) Velocity in the boundary layer. (c) Velocity at the base of the free troposphere. (d) Velocity at the top of the free troposphere. The flows in all the figures are shown in the carrier wave frame of reference, $-16.6\,\mathrm{ms}^{-1}$. For all of the solitary waves, the tropospheric flow vectors are plotted with the same scaling as are the boundary layer flow vectors, the latter being stretched to emphasize flow features.

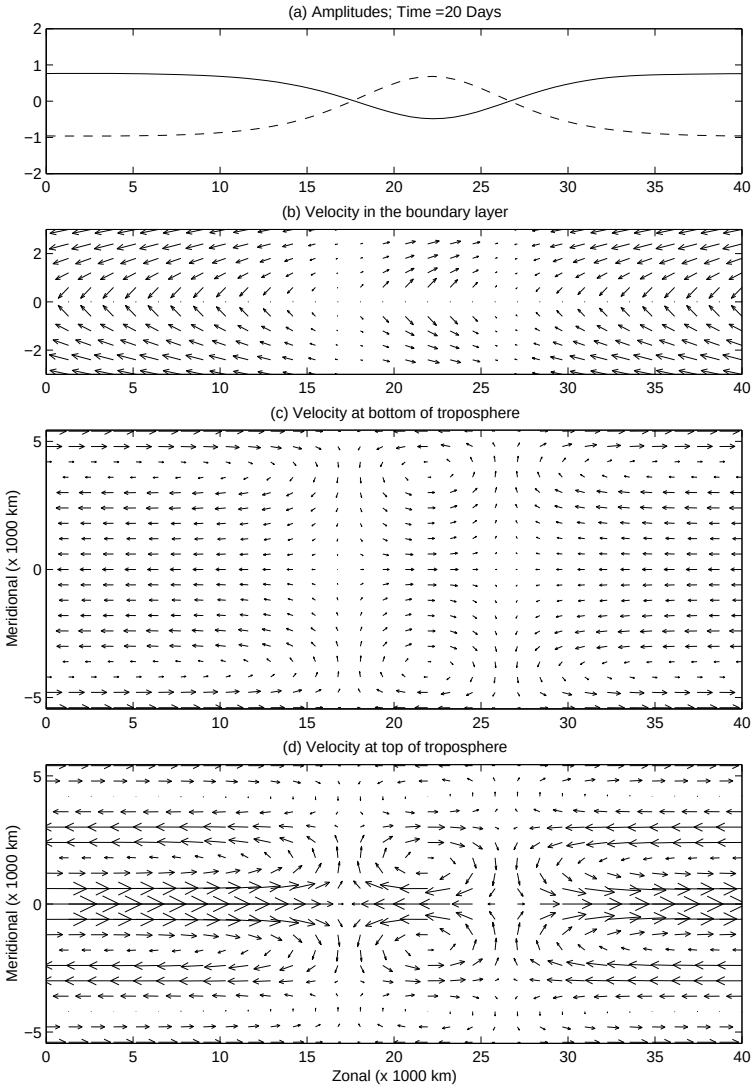


Fig. 10.— The solitary wave of figure 9 after 20 days. (a) Wave Amplitudes, solid - barotropic, dashed - baroclinic. (b) Velocity in the boundary layer. (c) Velocity at the base of the free troposphere. (d) Velocity at the top of the free troposphere.

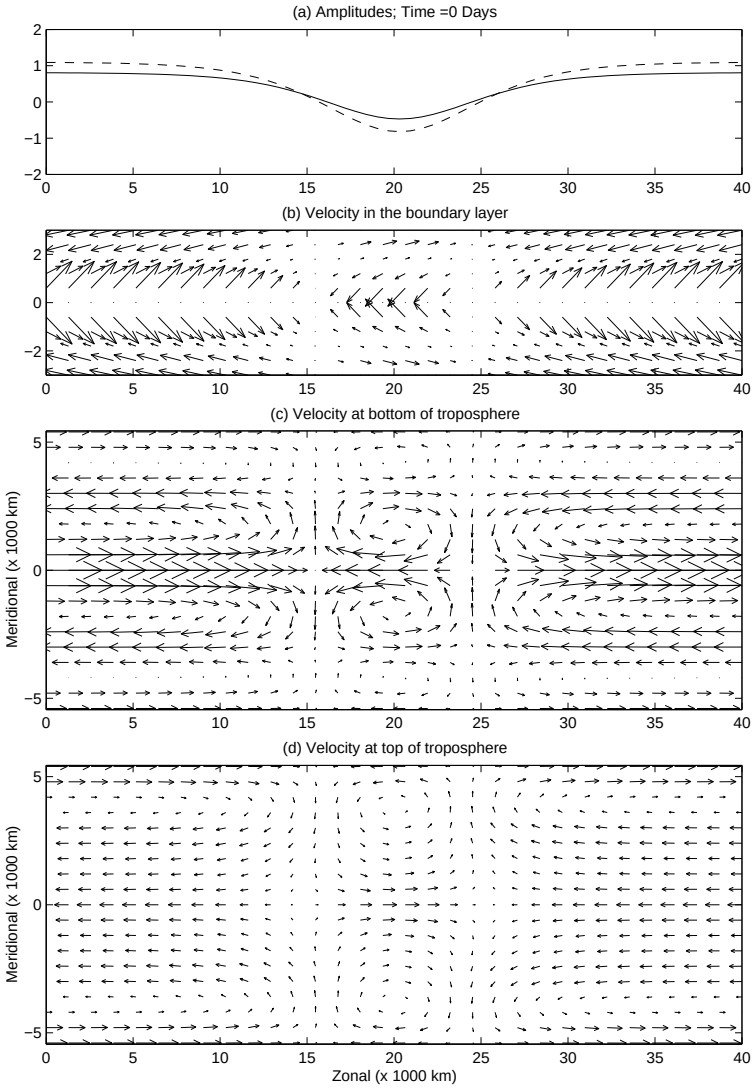


Fig. 11.— Initial condition for another 11400 km solitary wave traveling at $-15\,\mathrm{ms}^{-1}$. (a) Wave Amplitudes, solid - barotropic, dashed - baroclinic. (b) Velocity in the boundary layer. (c) Velocity at the base of the free troposphere. (d) Velocity at the top of the free troposphere.

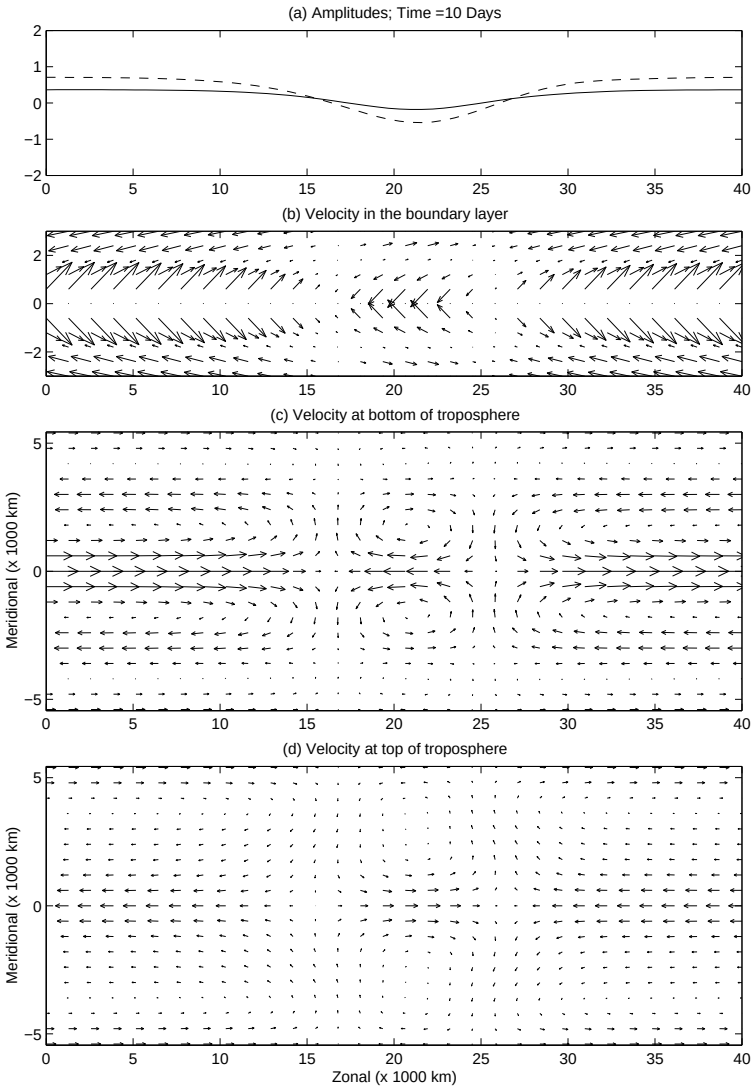


Fig. 12.— The remnants of the solitary wave of figure 11 after 10 days. The amplitudes are already greatly decayed and by 20 days are absolutely negligible. (a) Wave Amplitudes, solid - barotropic, dashed - baroclinic. (b) Velocity in the boundary layer. (c) Velocity at the base of the free troposphere. (d) Velocity at the top of the free troposphere.

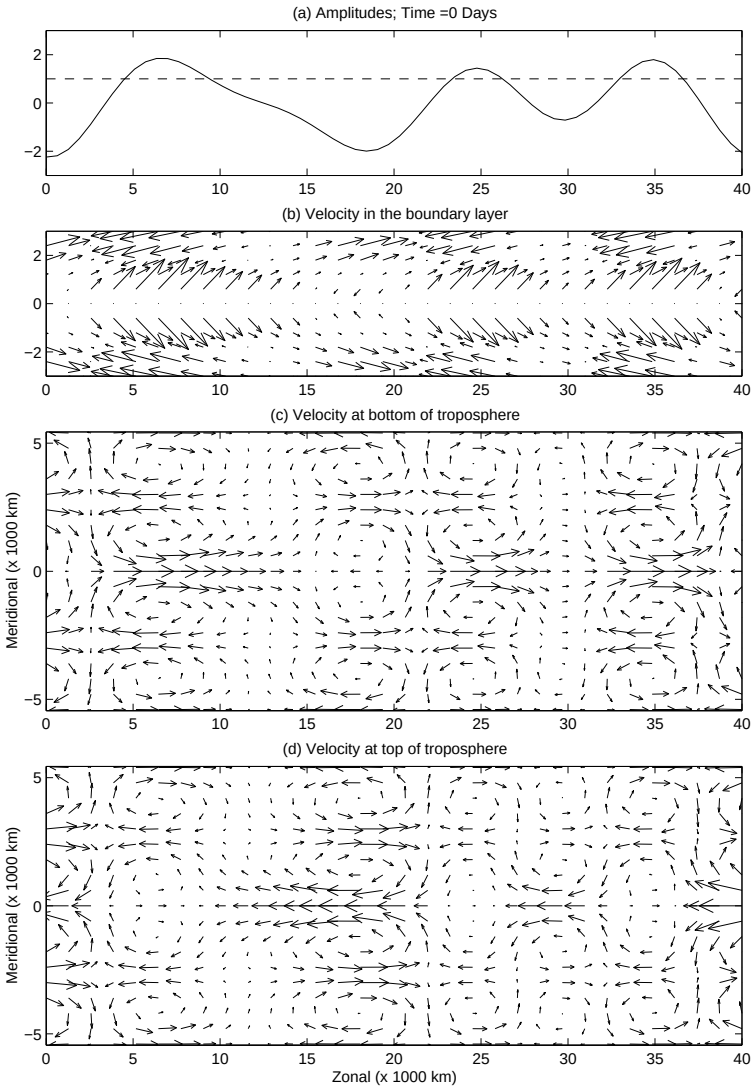


Fig. 13.— Initial velocity profile of a barotropic wave train with no initial barotropic mean wind and baroclinic mean shear of $5\,\mathrm{ms}^{-1}$. (a) Wave Amplitudes, solid - barotropic, dashed - baroclinic. (b) Velocity in the boundary layer. (c) Velocity at the base of the free troposphere. (d) Velocity at the top of the free troposphere.

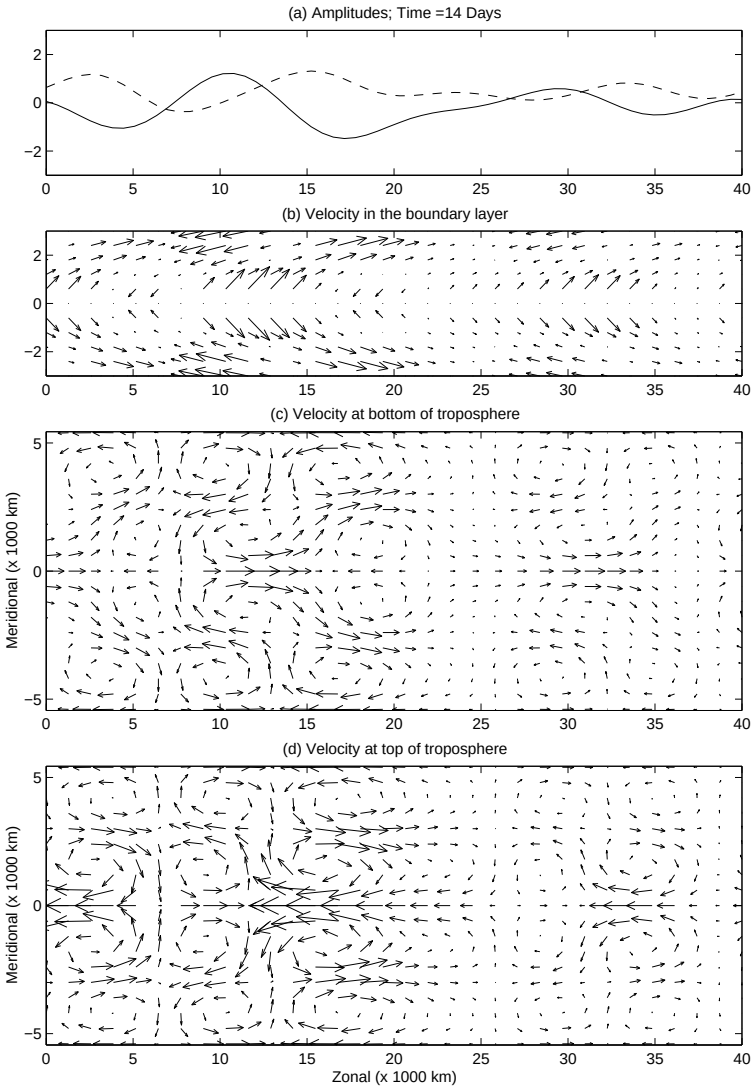


Fig. 14.— Velocity profile 14 days after an initially barotropic wave train with no initial barotropic mean wind and baroclinic mean shear of $5\,\mathrm{ms}^{-1}$. The "westerly wind burst"-like event persists despite both boundary layer and thermal dissipation dissipation. (a) Wave Amplitudes, solid - barotropic, dashed - baroclinic. (b) Velocity in the boundary layer. (c) Velocity at the base of the free troposphere. (d) Velocity at the top of the free troposphere.

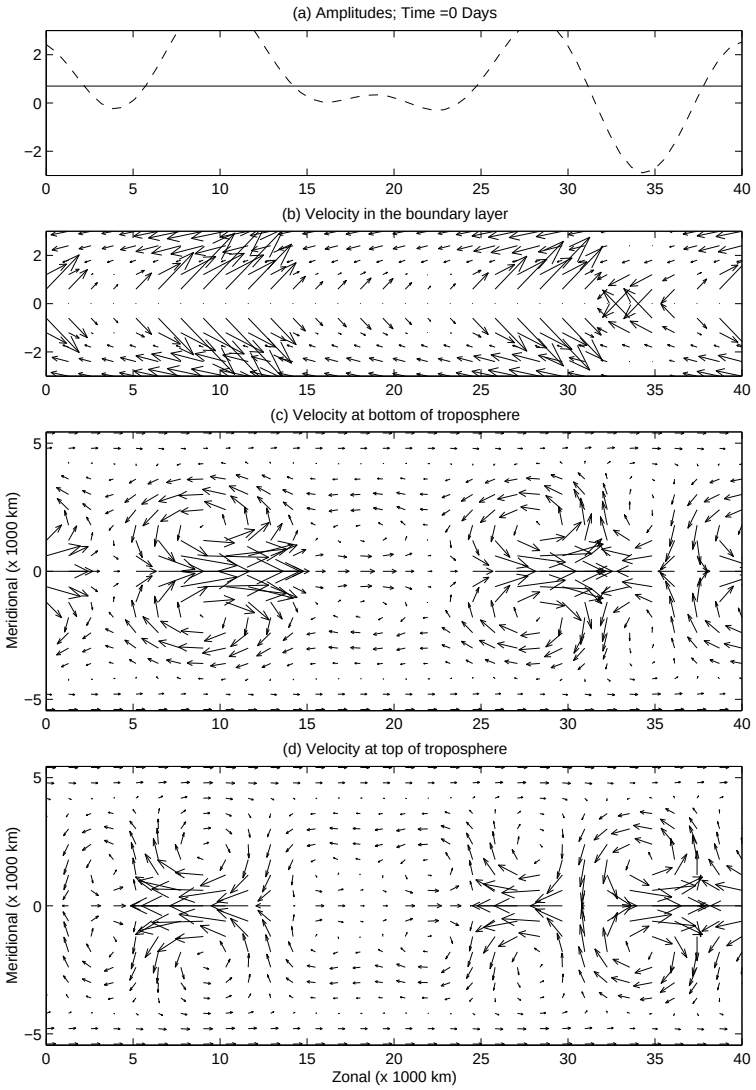


Fig. 15.— Initial velocity profile of a baroclinic wave train with barotropic mean wind of $2.5\,\mathrm{ms}^{-1}$ and baroclinic mean shear of $5\,\mathrm{ms}^{-1}$. (a) Wave Amplitudes, solid - barotropic, dashed - baroclinic. (b) Velocity in the boundary layer. (c) Velocity at the base of the free troposphere. (d) Velocity at the top of the free troposphere.

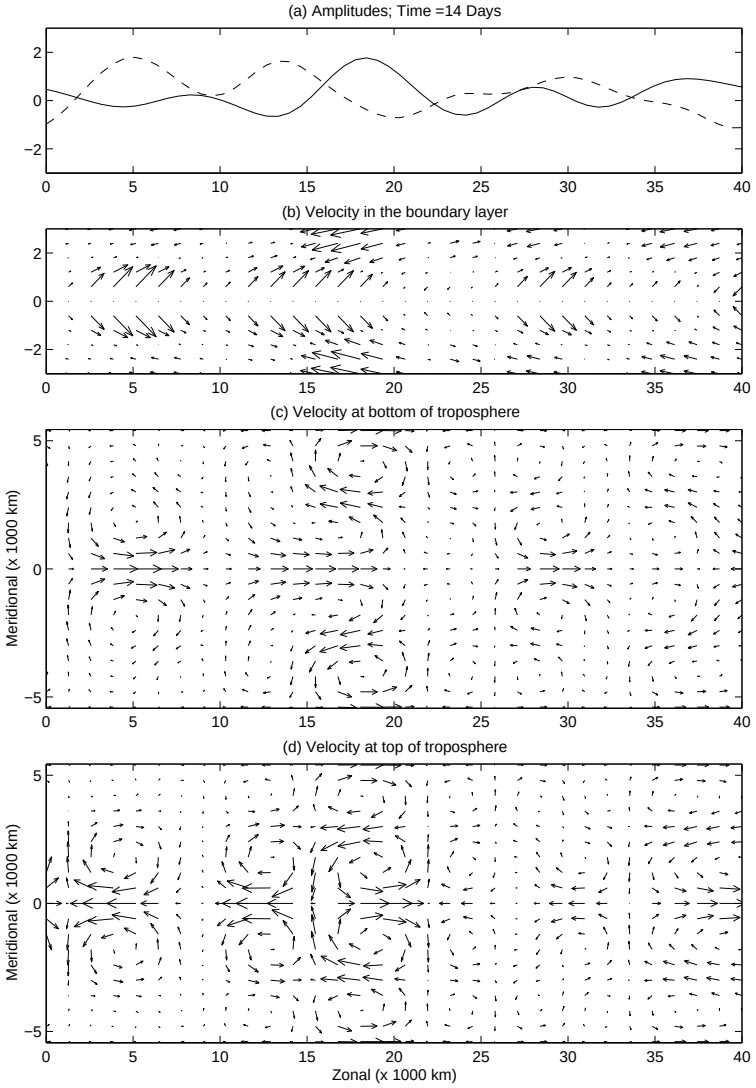


Fig. 16.— Velocity profile 14 days after an initially baroclinic wave train with barotropic mean wind of $2.5\,\mathrm{ms}^{-1}$ and baroclinic mean shear of $5\,\mathrm{ms}^{-1}$. A strong barotropic wave packet near $x = 20$ indicates that dissipation does not inhibit the conversion of baroclinic wave energy to barotropic wave energy. (a) Wave Amplitudes, solid - barotropic, dashed - baroclinic. (b) Velocity in the boundary layer. (c) Velocity at the base of the free troposphere. (d) Velocity at the top of the free troposphere.

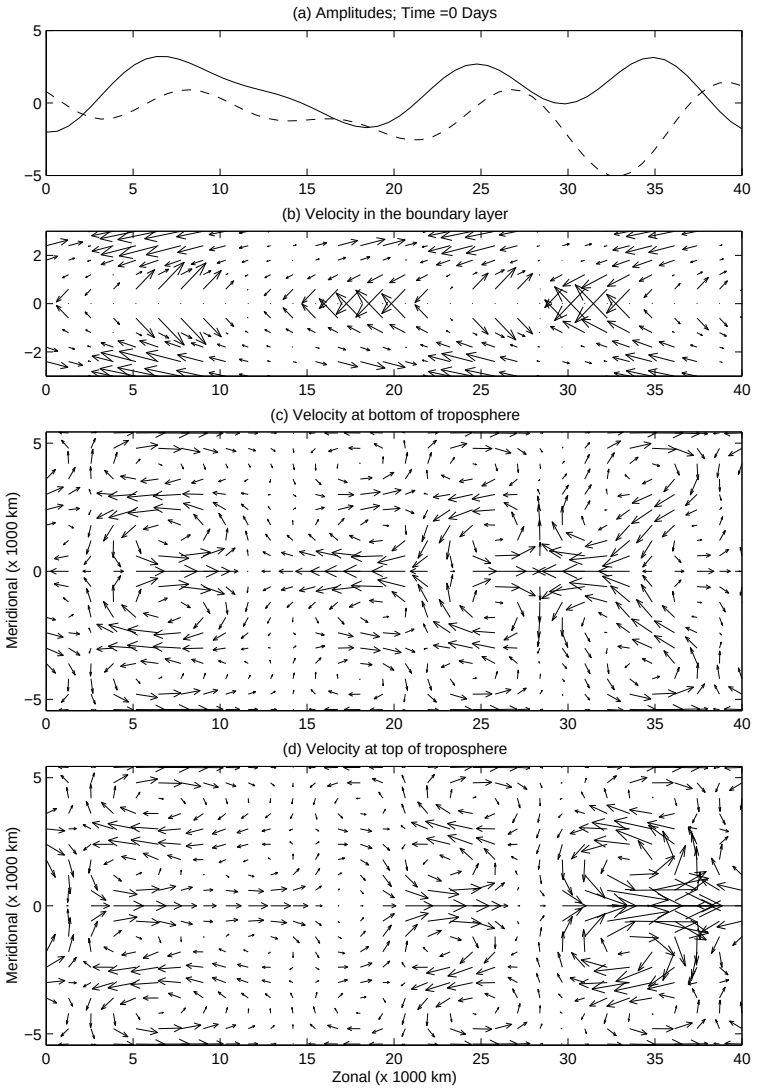


Fig. 17.— Random initial wave packet on a mean baroclinic shear of $-4.5\,\mathrm{ms}^{-1}$ and a mean barotropic wind of $3.1\,\mathrm{ms}^{-1}$, which are in a balanced state. (a) Wave Amplitudes, solid - barotropic, dashed - baroclinic. (b) Velocity in the boundary layer. (c) Velocity at the base of the free troposphere. (d) Velocity at the top of the free troposphere.

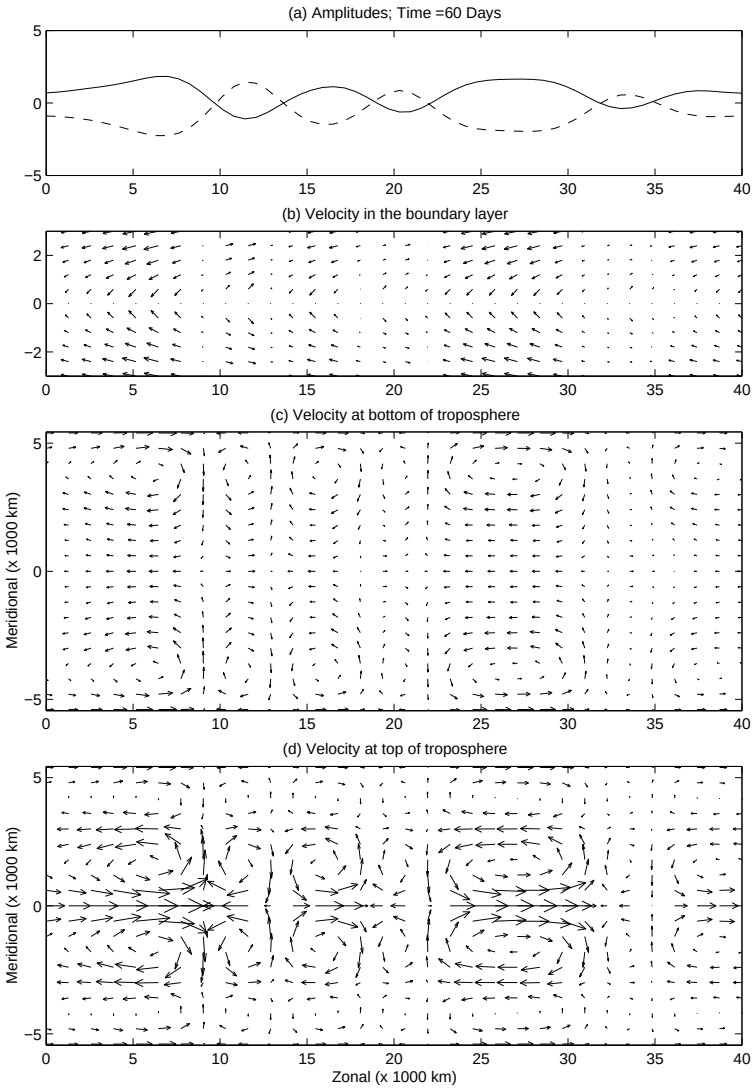


Fig. 18.— 60 days after figure 17 the waves become slaved to a slowly decaying state which is reminiscent of collection of solitary waves. (a) Wave Amplitudes, solid - barotropic, dashed - baroclinic. (b) Velocity in the boundary layer. (c) Velocity at the base of the free troposphere. (d) Velocity at the top of the free troposphere.